

## S3T stability of the homogeneous state of barotropic beta-plane turbulence

NIKOLAOS A. BAKAS, NAVID C. CONSTANTINOU\* AND PETROS J. IOANNOU

*Department of Physics, National and Kapodistrian University of Athens, Athens, Greece*

### ABSTRACT

Zonal jets and large scale non-zonal mean flows are often present in forced-dissipative barotropic turbulence on a beta-plane. The dynamics underlying the formation of both zonal and non-zonal coherent structures are investigated in this work within the statistical framework of Stochastic Structural Stability Theory (S3T). Previous studies using this framework have shown that the homogeneous turbulent state in barotropic beta-plane turbulence undergoes a bifurcation at a critical parameter and becomes inhomogeneous with the emergence of zonal jets and/or large scale non-zonal structures and that these predictions of S3T are verified by direct numerical simulations. In this paper, a systematic study of the dynamics underlying the S3T statistical instability of the homogeneous state for a wide range of parameters is presented. It is shown that for weak planetary vorticity gradient,  $\beta$ , both zonal jets and non-zonal large scale structures form from the upgradient momentum fluxes that result from the shearing of the eddies by the emerging infinitesimal large scale flow. For strong planetary vorticity gradient, the dynamics underlying the S3T instability were found to be different for zonal and non-zonal flows but in both cases the induced vorticity fluxes decrease with  $\beta$ . Shearing of the forced eddies by the mean flow continues to be the mechanism for the emergence of zonal jets while non-zonal large scale flows emerge from resonant and near resonant triad interactions between the large scale flow and the stochastically forced eddies.

### 1. Introduction

Atmospheric turbulence is commonly observed to be organized into slowly varying large scale structures such as zonal jets and coherent vortices. Prominent examples are the banded jets and the Great Red Spot in the Jovian atmosphere (Ingersoll 1990; Vasavada and Showman 2005). Laboratory experiments as well as direct numerical simulations of turbulent flows have shown that these coherent structures appear and persist for a very long time despite the presence of eddy mixing (Vallis and Maltrud 1993; Weeks et al. 1997; Read et al. 2004; Espa et al. 2010; Di Nitto et al. 2013).

A model that exhibits many aspects of turbulent self-organization into coherent structures yet is simple enough to extensively investigate, is a barotropic flow on the surface of a rotating planet or on a beta-plane with turbulence sustained by random stirring. Numerical simulations of this model have shown that robust zonal jets coexist with large scale westward propagating coherent waves (Sukoriansky et al. 2008; Galperin et al. 2010). These waves were found to either obey a Rossby wave dispersion, or

form non-dispersive packets that are referred to as satellite modes (Danilov and Gurarie 2004) or zonons (Sukoriansky et al. 2008). In addition, the formation of these coherent structures was shown to be a bifurcation phenomenon. As the energy input of the stochastic forcing is increased, the flow bifurcates from a turbulent, spatially homogeneous state to a state in which zonal jets and/or non-zonal coherent structures emerge and are maintained by turbulence (Bakas and Ioannou 2013a; Constantinou et al. 2014). In this work, we will address the eddy–mean flow dynamics underlying the emergence of both zonal and non-zonal structures.

Since organization of turbulence into coherent structures involves complex nonlinear interactions among a large number of degrees of freedom, an attractive approach is to study the statistical state dynamics of the flow, rather than single realizations of the turbulent field. That is, study the dynamics of the equations governing the evolution of the flow statistics, their fixed points which are statistical equilibria of the turbulent flow and their stability. This approach is followed in Stochastic Structural Stability Theory (S3T) (Farrell and Ioannou 2003) or Second Order Cumulant Expansion theory (CE2) (Marston et al. 2008), which is a non-equilibrium statistical theory that was applied to macroscale barotropic and baroclinic turbulence in planetary atmospheres (Farrell and Ioannou 2003, 2007, 2008; Marston et al. 2008; Farrell and Ioannou 2009a,b;

\*Corresponding author address: Navid Constantinou, University of Athens, Department of Physics, Section of Astrophysics, Astronomy and Mechanics, Build IV, Office 32, Panepistimiopolis, 15784 Zografos, Athens, Greece.

E-mail: navidcon@phys.uoa.gr

Marston 2010; Srinivasan and Young 2012; Marston 2012; Parker and Krommes 2013, 2014). This theory is based on two building blocks. The first is to form the equations governing the evolution of the flow statistics, which can be described by the cumulants of the flow. These cumulant equations govern the joint evolution of the mean flow (first cumulant) and the ensemble mean perturbation statistics (higher order cumulants). The second building block is to truncate the cumulant equations at second order by either parameterizing the terms involving the third cumulant (Farrell and Ioannou 1993a,b; DelSole and Farrell 1996; DelSole 2004) or setting the third cumulant to zero (Marston et al. 2008; Tobias et al. 2011; Srinivasan and Young 2012). Restriction of the dynamics to the first two cumulants is equivalent to neglecting the eddy-eddy interactions in the fully nonlinear dynamics and retaining only the interaction between the eddies with the instantaneous mean flow. This second order closure results in a nonlinear, autonomous dynamical system that governs the evolution of the mean flow and its consistent second order perturbation statistics. Its fixed points define statistical equilibria, whose instability brings about structural reconfiguration of the mean flow and the turbulent statistics.

Previous studies employing S3T addressed the bifurcation from a homogeneous turbulent regime to a jet forming regime in barotropic beta-plane turbulence and identified the emerging jet structures as linearly unstable modes to the homogeneous turbulent state equilibrium (Farrell and Ioannou 2003, 2007; Bakas and Ioannou 2011; Srinivasan and Young 2012; Parker and Krommes 2013, 2014). Comparison of the results of the stability analysis with direct numerical simulations have shown that the structure of zonal flows that emerge in the nonlinear simulations can be predicted by S3T (Srinivasan and Young 2012; Constantinou et al. 2014). These studies however assumed that the ensemble average over the forcing realizations is equivalent to a zonal average. Under this simplification, the non-zonal structures are treated as incoherent and their emergence and effect on the jet dynamics cannot be addressed. In recent studies, an alternative ergodic assumption was made. The ensemble average was assumed to be equivalent to a Reynolds average over the fast turbulent motions (Bernstein 2009; Bernstein and Farrell 2010). With this definition of the ensemble mean, Bakas and Ioannou (2013a, 2014) addressed the emergence of non-zonal coherent structures in barotropic beta-plane turbulence in terms of the parameters  $\beta^* = \beta/(rL_f^{-1})$  and  $\varepsilon^* = \varepsilon/(r^3L_f^2)$  where  $\beta$  is the gradient of the planetary vorticity,  $L_f$  the length-scale of the forcing,  $\varepsilon$  the energy input rate of the forcing and  $1/r$  the dissipation time-scale. It was found that for isotropic forcing the homogeneous statistical equilibrium becomes unstable when the energy input rate exceeds a critical value  $\varepsilon_c^*$  that depends on  $\beta^*$  as shown in Fig. 1. When  $\beta^* \ll 1$ , zonal jets are more unstable than non-zonal structures and are expected

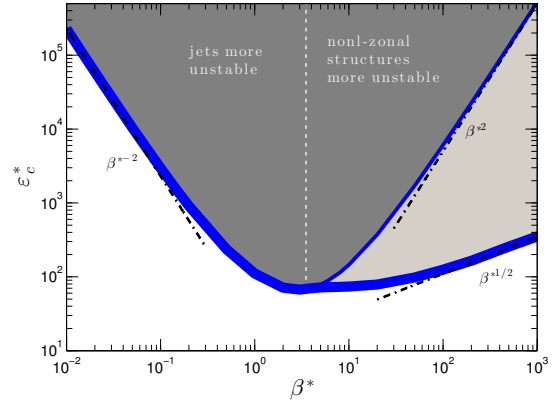


FIG. 1. The non-dimensional critical energy input rate  $\varepsilon_c^*$  for S3T instability (thick solid line) and the critical energy input rate for S3T instability of zonal jets (solid line) as a function of the non-dimensional planetary vorticity gradient,  $\beta^*$ , for isotropic stochastic forcing. For  $\beta^* \gg 1$  the critical energy input rate for the emergence of jets increases as  $\varepsilon_c^* \sim \beta^{*2}$ , while for the formation of non-zonal structures it increases as  $\varepsilon_c^* \sim \beta^{*1/2}$ . In the light shaded region only non-zonal coherent structures emerge, while in the dark shaded region both zonal jets and non-zonal coherent structures emerge. The thin dotted vertical line  $\beta^* = \beta_{\min}^*$  separates the unstable region: for  $\beta^* < \beta_{\min}^*$  zonal structures grow the most, whereas for  $\beta^* > \beta_{\min}^*$  non-zonal structures grow the most. Maximum instability occurs for  $\beta^* \approx 3$ .

to form. When  $\beta^* \gg 1$ , westward propagating non-zonal structures are more unstable than zonal jets. In this case, integrations of the S3T system have shown that the most unstable structures emerge and equilibrate at low supercriticalities to finite amplitude traveling waves. At larger energy input rates, the finite amplitude non-zonal traveling states are unstable and the flow equilibrates to mixed zonal jet-traveling wave states that consist of strong zonal jets with weaker traveling non-zonal structures embedded in them. These predictions of the S3T stability analysis were verified by direct numerical simulations of the turbulent barotropic flow (Bakas and Ioannou 2014).

The S3T dynamics that underlie the formation of large scale structure can not depend on turbulent anisotropic inverse cascade processes because local in wavenumber space eddy-eddy interactions are absent in S3T. In S3T, large scale structure emerges from a cooperative instability arising from the non-local in wavenumber space interaction between the large scale mean flow and the forced, small scale turbulent eddies. The eddy-mean flow dynamics of this cooperative instability has been investigated by Bakas and Ioannou (2013b) for the case of zonal jet emergence in the limit of  $\beta^* \ll 1$ . It was shown that shear straining of the small scale eddies by the local shear of an infinitesimal sinusoidal zonal jet, as described by Orr dynamics in a beta-plane, produces upgradient fluxes that intensify in general the zonal jet. In this work we will

extend the study of this cooperative eddy–mean flow instability to address not only zonal jet formation but also formation of non-zonal coherent structures. Moreover, we will also address the formation of coherent structures for a wide range of values of  $\beta^*$ .

This paper is organized as follows. In section 2 we derive the S3T system for a barotropic flow and the resulting eigenvalue problem addressing the stability of the homogeneous statistical equilibrium. In section 3 we transform the eigenvalue problem in a rotated frame of reference, so that the formation of zonal jets and non-zonal structures can be studied under a uniform framework. In section 4 we identify the eddy–mean flow dynamics underlying the S3T instability for isotropic stochastic forcing and in section 5 we study the effect of the forcing anisotropy to the S3T instability. Finally, a brief discussion of the obtained results and our conclusions is made in section 6.

## 2. Formulation of S3T dynamics and emergence of non-zonal coherent structures

Consider a barotropic flow on an infinite beta-plane with  $x$  and  $y$  Cartesian coordinates along the zonal and the meridional direction respectively and with planetary vorticity gradient,  $\beta = (0, \beta)$ . The non-divergent velocity field is expressed in terms of a streamfunction,  $\psi$ , as  $\mathbf{u} = (u, v) = (-\partial_y \psi, \partial_x \psi)$ . The vorticity of the fluid  $\zeta = \partial_x v - \partial_y u = \Delta \psi$ , with  $\Delta \equiv \partial_{xx}^2 + \partial_{yy}^2$ , evolves as:

$$\partial_t \zeta + J(\psi, \zeta + \beta \cdot \mathbf{x}) = -r\zeta + \sqrt{\varepsilon} \xi, \quad (1)$$

where  $\mathbf{x} = (x, y)$  and  $J$  is the two dimensional Jacobian,  $J(A, B) \equiv (\partial_x A)(\partial_y B) - (\partial_y A)(\partial_x B)$ . The flow is dissipated with linear damping at a rate  $r$ , which typically models Ekman drag in planetary atmospheres. Turbulence is maintained by the external stochastic forcing,  $\xi$ , which models exogenous processes, such as turbulent convection or energy injected by baroclinic instability. We assume that  $\sqrt{\varepsilon} \xi(\mathbf{x}, t)$  is a temporally delta-correlated and spatially homogeneous random stirring that injects energy at a rate  $\varepsilon$ . We non-dimensionalize (1) using the dissipation time-scale  $1/r$  and the typical length-scale of the stochastic excitation,  $L_f$ . In these units  $\zeta^* = \zeta/r$ ,  $\psi^* = \psi/(rL_f^2)$ ,  $\beta^* = \beta/(rL_f^{-1})$ ,  $\varepsilon^* = \varepsilon/(r^3 L_f^2)$ ,  $\xi^* = \xi/(r^{1/2} L_f^{-1})$  and  $r^* = 1$  where the asterisks denote non-dimensional variables and we hereafter drop the asterisks for simplicity.

To construct the S3T dynamical system for the evolution of the flow statistics we adopt the continuous formulation of [Srinivasan and Young \(2012\)](#) and proceed as follows:

1. We decompose the vorticity field into the averaged field,  $Z = \mathcal{T}[\zeta]$ , defined as a time average over an intermediate time scale and deviations from the mean or eddies,  $\zeta' = \zeta - Z$ . The intermediate time scale is

larger than the time scale of the turbulent motions but smaller than the time scale of the large scale motions. With this decomposition we rewrite (1) as:

$$\partial_t Z + J(\Psi, Z + \beta \cdot \mathbf{x}) = -\mathcal{T}[J(\psi', \zeta')] - Z, \quad (2a)$$

$$\begin{aligned} \partial_t \zeta' = & \underbrace{-J(\psi', Z + \beta \cdot \mathbf{x}) - J(\Psi, \zeta') - \zeta'}_{\mathcal{A}(\mathbf{U})\zeta'} + \underbrace{\mathcal{T}[J(\psi', \zeta')] - J(\psi', \zeta')}_{f_{\text{NL}}} + \sqrt{\varepsilon} \xi, \end{aligned} \quad (2b)$$

where  $\Psi = \mathcal{T}[\psi]$  and  $\mathcal{A}(\mathbf{U}) \equiv -\mathbf{U} \cdot \nabla + [(\Delta \mathbf{U}) \cdot \nabla + \hat{\mathbf{z}} \cdot (\beta \times \nabla)] \Delta^{-1} - 1$  is the operator that governs the linear evolution of perturbations to the instantaneous mean flow  $\mathbf{U} = (U, V) = (-\partial_y \Psi, \partial_x \Psi)$ . As in previous studies ([Farrell and Ioannou 2003](#); [Srinivasan and Young 2012](#); [Bakas and Ioannou 2014](#)), we neglect the eddy-eddy term  $f_{\text{NL}} \equiv \mathcal{T}[J(\psi', \zeta')] - J(\psi', \zeta')$  to obtain the quasi-linear system,

$$\partial_t Z + J(\Psi, Z + \beta \cdot \mathbf{x}) = -\mathcal{T}[J(\psi', \zeta')] - Z, \quad (3a)$$

$$\partial_t \zeta' = \mathcal{A}(\mathbf{U})\zeta' + \sqrt{\varepsilon} \xi. \quad (3b)$$

2. In order to obtain the statistical dynamics of the quasi-linear system (3) we make the ergodic assumption that the time average over the intermediate time scale is equal to the ensemble average over the forcing realizations. Under this assumption, the slowly varying mean flow  $Z$  is also the first cumulant of the vorticity  $Z = \langle \zeta \rangle$ , where the brackets denote the ensemble average. In addition, the time mean of the vorticity flux divergence is equal to the ensemble mean of the flux divergence,  $\mathcal{T}[J(\psi', \zeta')] = \langle J(\psi', \zeta') \rangle$ , which can be expressed as a linear function,  $\mathcal{R}(C)$ , of the eddy vorticity covariance between points  $\mathbf{x}_a$  and  $\mathbf{x}_b$ ,

$$C(\mathbf{x}_a, \mathbf{x}_b, t) = \langle \zeta'(\mathbf{x}_a, t) \zeta'(\mathbf{x}_b, t) \rangle, \quad (4)$$

with

$$\begin{aligned} \mathcal{R}(C) \equiv & -\partial_x \left[ -\frac{1}{2} (\Delta_a^{-1} \partial_{y_a} + \Delta_b^{-1} \partial_{y_b}) C \right]_{\mathbf{x}_a = \mathbf{x}_b} - \\ & -\partial_y \left[ \frac{1}{2} (\Delta_a^{-1} \partial_{x_a} + \Delta_b^{-1} \partial_{x_b}) C \right]_{\mathbf{x}_a = \mathbf{x}_b} \\ = & -\langle J(\psi', \zeta') \rangle. \end{aligned} \quad (5)$$

The subscript  $a$  or  $b$  in operators denotes hereafter the action of the operators only on the variables  $\mathbf{x}_a$  or  $\mathbf{x}_b$  and with the subscript  $\mathbf{x}_a = \mathbf{x}_b$  we denote that any expression depending on the two variables  $\mathbf{x}_a$  and  $\mathbf{x}_b$  is evaluated at  $\mathbf{x}_a = \mathbf{x}_b$ .

3. The first cumulant,  $Z$ , evolves according to:

$$\partial_t Z + J(\Psi, Z + \beta \cdot \mathbf{x}) = \mathcal{R}(C) - Z. \quad (6a)$$

By taking the time derivative of (4) and using (3b) we obtain the evolution equation for the second cumulant  $C$ :

$$\partial_t C = [\mathcal{A}_a(\mathbf{U}) + \mathcal{A}_b(\mathbf{U})] C + \varepsilon Q, \quad (6b)$$

where  $Q(\mathbf{x}_a, \mathbf{x}_b) = Q(\mathbf{x}_a - \mathbf{x}_b)$  is the spatial covariance of the homogeneous stochastic forcing<sup>1</sup> and  $\mathcal{A}_a(\mathbf{U})$  implies that the coefficients of  $\mathcal{A}(\mathbf{U})$  are evaluated at  $\mathbf{x}_a$  and that it acts only on the variable  $\mathbf{x}_a$ .

Equations (6) comprise the autonomous S3T system which constitutes a second-order closure for the flow statistics. Being autonomous it may possess statistical equilibria ( $Z^e, C^e$ ), the stability of which is addressed by considering small perturbations ( $\delta Z, \delta C$ ) and performing an eigenanalysis of the linearized S3T equations about these equilibria.

For spatially homogeneous forcing,

$$Z^e = 0, \quad C^e = \frac{\varepsilon}{2} Q, \quad (7)$$

is a statistical equilibrium of the S3T system with no mean flow and a homogeneous eddy field, i.e. with a translationally invariant covariance,  $C^e(\mathbf{x}_a - \mathbf{x}_b)$ . The linearized S3T equations about (7) are:

$$\partial_t \delta Z + J(\delta \Psi, \beta \cdot \mathbf{x}) = \mathcal{R}(\delta C) - \delta Z, \quad (8a)$$

$$\partial_t \delta C = (\mathcal{A}_a^e + \mathcal{A}_b^e) \delta C + (\delta \mathcal{A}_a + \delta \mathcal{A}_b) C^e, \quad (8b)$$

where  $\mathcal{A}_j^e \equiv \mathcal{A}_j(\mathbf{U}^e)$  and  $\delta \mathcal{A}_j \equiv \mathcal{A}_j(\mathbf{U}^e + \delta \mathbf{U}) - \mathcal{A}_j^e$ ,  $j = a, b$ . From (8) it can be found that equilibrium (7) is S3T stable for  $\varepsilon < \varepsilon_c$  and becomes unstable when  $\varepsilon$  exceeds the critical value  $\varepsilon_c$ , which depends both on  $\beta$  and on the spectral structure of the forcing. Previous studies have shown that the unstable structures identified through the S3T stability analysis are in close correspondence with the coherent structures that emerge in nonlinear simulations of the turbulent flow. In this work we investigate the eddy–mean flow dynamics underlying the S3T instability of the homogeneous flow and identify the physical processes underlying the instability. We follow [Srinivasan and Young \(2014\)](#) and consider a stochastic forcing that

injects energy on a narrow ring in wavenumber space with power spectrum

$$\hat{Q}(\mathbf{k}) = \iint_{-\infty}^{+\infty} Q(\mathbf{x}_a - \mathbf{x}_b) e^{-i\mathbf{k} \cdot (\mathbf{x}_a - \mathbf{x}_b)} d(x_a - x_b) d(y_a - y_b) \\ = 4\pi \delta(k-1) \mathcal{G}(\vartheta), \quad (9)$$

where  $\mathbf{k} = (k_x, k_y)$ ,  $k = |\mathbf{k}|$ ,  $\vartheta = \arctan(k_y/k_x)$  and

$$\mathcal{G}(\vartheta) = 1 + \mu \cos(2\vartheta). \quad (10)$$

The parameter  $\mu$  measures the anisotropy of the forcing and satisfies  $-1 \leq \mu \leq 1$ , so that the covariance power spectrum is always positive. The typical structure of the forcing covariance spectrum and of the realization of the stochastic excitation for different values of  $\mu$  are shown in Fig. 2. When  $\mu = 0$ , the forcing is isotropic and could model sources like turbulent convection. When  $\mu > 0$ , the stochastic excitation injects larger power at Fourier components with  $k_y = 0$ , which resemble the most unstable baroclinic mode. Both cases have been considered in previous studies of S3T ([Farrell and Ioannou 2007](#); [Bakas and Ioannou 2011](#); [Srinivasan and Young 2012](#); [Constantinou et al. 2014](#)). When  $\mu < 0$ , the forcing injects larger power at almost zonal Fourier components with  $k_x = 0$ .

### 3. Emergence of non-zonal structures as zonal flows in a rotated frame

The eigenfunctions of the S3T stability equations (8) are specified by their two components: the mean flow component  $\delta \tilde{Z} e^{\sigma t}$ , and the covariance component  $\delta \tilde{C} e^{\sigma t}$ . Because the stability equations (8) are linearized about the homogeneous equilibrium (7), the eigenfunction structure simplifies significantly and assumes the form:

$$\delta \tilde{Z}(\mathbf{x}) = e^{i\mathbf{n} \cdot \mathbf{x}}, \quad (11a)$$

$$\delta \tilde{C}(\mathbf{x}_a, \mathbf{x}_b) = \tilde{C}_{\mathbf{n}}^{(h)}(\mathbf{x}_a - \mathbf{x}_b) e^{i\mathbf{n} \cdot (\mathbf{x}_a + \mathbf{x}_b)/2}. \quad (11b)$$

where  $\mathbf{n} = (n_x, n_y)$  is the wavevector that characterizes the eigenfunction and  $\tilde{C}_{\mathbf{n}}^{(h)}(\mathbf{x}_a - \mathbf{x}_b)$  is the homogeneous component of the covariance eigenfunction. The mean flow component of each eigenfunction has the form of a zonal flow when  $n_x = 0$  and of a non-zonal flow when  $n_x \neq 0$ . However, non-zonal mean flow perturbations can be rendered zonal through a rotation of the frame of reference.

For an eigenfunction with wavenumber  $\mathbf{n}$ , clockwise rotation of the axes by an angle  $\varphi = \arctan(n_x/n_y)$  transforms the components of  $\mathbf{n}$  to:

$$n'_x = n_x \cos \varphi - n_y \sin \varphi = 0, \quad n'_y = n_x \sin \varphi + n_y \cos \varphi = n, \quad (12)$$

where  $n = |\mathbf{n}|$ , and also transforms the planetary vorticity gradient components to  $\beta = (-\beta \sin \varphi, \beta \cos \varphi)$ . Correspondingly, in the rotated frame the eigenfunction has

<sup>1</sup> $Q$  is defined through  $\langle \xi(\mathbf{x}_a, t) \xi(\mathbf{x}_b, t') \rangle = Q(\mathbf{x}_a - \mathbf{x}_b) \delta(t - t')$  and it is an even function of  $\mathbf{x}_a - \mathbf{x}_b$  since  $\langle \xi(\mathbf{x}_a, t) \xi(\mathbf{x}_b, t') \rangle = \langle \xi(\mathbf{x}_b, t) \xi(\mathbf{x}_a, t') \rangle$ .

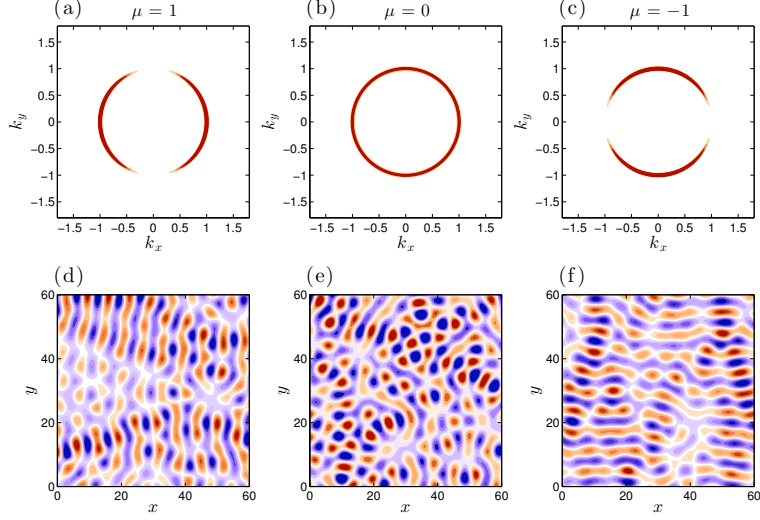


FIG. 2. Top panels show the forcing covariance spectrum,  $\hat{Q}(\mathbf{k}) = 4\pi\delta(k-1) \times [1 + \mu \cos(2\vartheta)]$ , for (a)  $\mu = 1$ , (b)  $\mu = 0$  and (c)  $\mu = -1$  (the delta function is represented with a finite thickness ring). Bottom panels show vorticity field contours of a stochastic forcing realization for (d)  $\mu = 1$ , (e)  $\mu = 0$  and (f)  $\mu = -1$ .

only the mean flow component  $\delta\tilde{U}(y')$ , which is of the form of a zonal jet in the  $x'$  direction (cf. Fig. 3), with  $\delta\tilde{Z} = -\partial_{y'}\delta\tilde{U}$ , and the eigenvalue problem (8) about the homogeneous equilibrium transforms to<sup>2</sup>:

$$\sigma \partial_{y'} \delta\tilde{U} = -\beta \sin \varphi \delta\tilde{U} - \partial_{y'} \delta\tilde{U} + \partial_{y'} (\delta \langle v' \zeta' \rangle), \quad (13a)$$

$$\sigma \delta\tilde{C} = (\mathcal{A}_a^{e'} + \mathcal{A}_b^{e'}) \delta\tilde{C} + (\delta\mathcal{A}_a^{e'} + \delta\mathcal{A}_b^{e'}) C^{e'}, \quad (13b)$$

with  $\mathcal{A}^{e'} \equiv -(\beta \sin \varphi \partial_{y'} + \beta \cos \varphi \partial_{x'}) \Delta^{-1} - 1$  and  $\delta\mathcal{A}^{e'} = -\delta\tilde{U} \partial_{x'} + (\partial_{y'}^2 \delta\tilde{U}) \partial_{x'} \Delta^{-1}$ .  $C^{e'}$  is the equilibrium covariance in the rotated frame of reference which when considered as a function of the components of the coordinates satisfies  $C^{e'}(x'_a - x'_b, y'_a - y'_b) = C^e(x_a - x_b, y_a - y_b)$ , where  $(x'_a, y'_a)$  are the components of  $\mathbf{x}_a$  in the rotated frame. The spatial structure of the perturbation vorticity flux  $\delta \langle v' \zeta' \rangle$  is given in terms of  $\delta C$  as:

$$\delta \langle v' \zeta' \rangle = \left[ \frac{1}{2} (\Delta_a^{-1} \partial_{x'_a} + \Delta_b^{-1} \partial_{x'_b}) \delta\tilde{C} \right]_{\mathbf{x}_a = \mathbf{x}_b}. \quad (14)$$

In writing the S3T eigenvalue problem in the rotated frame and by transforming a non-zonal perturbation into a zonal jet perturbation there is a twofold gain. The first is that we can use the methods that were previously developed by [Bakas and Ioannou \(2013b\)](#) in the context of the emergence of zonal jets in order to understand the mechanisms responsible for the emergence of non-zonal structures. The second, is that we can directly address the eddy–mean flow dynamics that give rise to zonal jets in cases where the effect of topography is equivalent to a tilted planetary

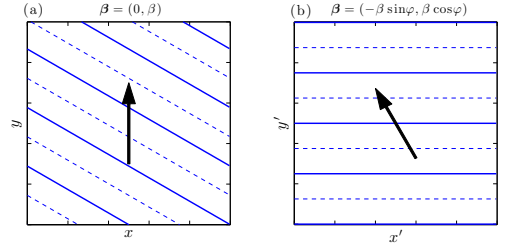


FIG. 3. (a) Constant phase lines of a non-zonal mean flow eigenfunction  $\delta\tilde{Z} = e^{i\mathbf{m}\cdot\mathbf{x}}$  with  $\varphi = \arctan(n_x/n_y) = 30^\circ$ . The arrow shows the direction of planetary vorticity gradient  $\beta = (0, \beta)$ . (b) Same as (a) but in a frame which has been rotated clockwise by angle  $\varphi$ , so that  $\delta\tilde{Z} = e^{i\mathbf{m}'\cdot\mathbf{x}'}$ . The arrow shows the direction of the planetary vorticity gradient  $\beta = (-\beta \sin \varphi, \beta \cos \varphi)$  in the rotated frame.

vorticity gradient, such as the case of a slanted ocean bed considered by [Boland et al. \(2012\)](#).

From hereafter we will study S3T instability of (7) through (13). While in the rotated frame of reference all eigenfunctions have the form of a zonal jet, we refer to the case of  $\varphi = 0$  as corresponding to zonal jets, and to the case  $\varphi \neq 0$  as corresponding to non-zonal structures, as they would be characterized in the unrotated frame. If (13a) admits a solution by eigenfunction  $\delta\tilde{U}$  and  $\delta\tilde{C}$ , then the vorticity flux,  $\delta \langle v' \zeta' \rangle$ , must also be itself proportional to the mean flow perturbation eigenfunction  $\delta\tilde{U}$ , i.e. we must have

$$\delta \langle v' \zeta' \rangle = \varepsilon f(\sigma) \delta\tilde{U}, \quad (15)$$

where the proportionality constant  $f$  is the vorticity flux feedback induced by the mean flow eigenfunction  $\delta\tilde{U}$  with

<sup>2</sup>  $\delta\tilde{V}(y') = 0$  in the rotated frame due to continuity.



eigenvalue  $\sigma$ . With this notation we show in 6 Appendix A that the stability equation which determines the eigenvalue  $\sigma$  is:

$$\sigma + 1 - i\beta \sin \varphi / n = \varepsilon f(\sigma), \quad (16)$$

where

$$f(\sigma) = \iint_{-\infty}^{+\infty} \frac{dk_x dk_y}{(2\pi)^2} [2nk_x^2(k_y + n/2)(k^2 - n^2)] \times \\ \times [(\sigma + 2)k_s^2 k^2 + 2in\beta \cos \varphi k_x(k_y + n/2) \\ - in\beta \sin \varphi (k_x^2 - k_y^2 - nk_y)]^{-1} \times \frac{\hat{Q}'(k_x, k_y)}{2}, \quad (17)$$

with  $\mathbf{k}_s = \mathbf{k} + \mathbf{n}$ ,  $k_s = |\mathbf{k}_s|$  and

$$\hat{Q}'(k_x, k_y) = 4\pi \delta(k - 1) \mathcal{G}(\vartheta - \varphi), \quad (18)$$

the Fourier transform of  $Q$  in the rotated frame. For  $\varphi = 0$ , (16) reduces to the eigenvalue relation of [Srinivasan and Young \(2012\)](#) that governs the stability of the homogeneous equilibrium (7) to zonal jet perturbations in the unrotated frame. When these zonal jet eigenfunctions have positive growth rate ( $\sigma_r \equiv \text{Re}(\sigma) > 0$ ), the jets grow without translating (i.e.  $\sigma_i \equiv \text{Im}(\sigma) = 0$ ) for the specified forcing. For  $\varphi \neq 0$  the above expression produces the eigenvalue relation obtained by [Bakas and Ioannou \(2014\)](#) for the growth rate of non-zonal perturbations with wavenumbers  $(n_x, n_y) = (n \sin \varphi, n \cos \varphi)$  in the unrotated frame. The growing eigenfunctions in this case are typically propagating in the retrograde direction and for  $\beta \gg 1$  and close to the stability boundary their frequency  $\sigma_i$  is given as  $\sigma_i = -\omega_n$ , where

$$\omega_n \equiv \frac{\hat{\mathbf{z}} \cdot (\boldsymbol{\beta} \times \mathbf{n})}{n^2}, \quad (19)$$

is the Rossby wave frequency corresponding to wavevector  $\mathbf{n}$ .

From (16), one obtains that instability occurs only if the real part of the vorticity flux feedback factor  $f_r \equiv \text{Re}(f)$  is positive. If this condition is satisfied, the induced vorticity fluxes are upgradient and the homogeneous equilibrium is unstable for  $\varepsilon > \varepsilon_c \equiv 1/f_r$ . In order to illuminate the eddy-mean flow dynamics underlying the S3T instability, we study the behavior of  $f_r$  as a function of parameters for excitation amplitudes close to  $\varepsilon_c$ . Near the stability boundary  $\sigma_r \approx 0$  and under the assumption that at marginal stability<sup>3</sup>  $\sigma_i \approx -\omega_n = \beta \sin \varphi / n$ , the feedback on the mean

flow perturbation with wavenumber  $n$  for forcing (18) can be written as:

$$f_r = \int_0^\pi \mathcal{F}(\vartheta, n) d\vartheta, \quad (20)$$

where  $\mathcal{F}(\vartheta, n)$  is the contribution to  $f_r$  from the individual Fourier components of the forcing. The integrand  $\mathcal{F}(\vartheta, n)$  can be alternatively interpreted as the contribution of the stochastically forced waves or eddies to the vorticity fluxes. These forced waves have for the narrow band ring forcing a total wavenumber  $k = 1$  and are characterized only by the angle  $\vartheta$  between their phase lines and the  $y$  axis. We can isolate the dependence of the feedback factor on  $\beta$  by writing  $\mathcal{F}(\vartheta, n) = F(\vartheta, n) + F(180^\circ + \vartheta, n)$  with

$$F(\vartheta, n) = \frac{\mathcal{N} \mathcal{D}_0}{\mathcal{D}_0^2 + \beta^2 \mathcal{D}_2^2}, \quad (21)$$

where, as shown in Appendix A, functions  $\mathcal{N}$ ,  $\mathcal{D}_0$ ,  $\mathcal{D}_2$  do not depend on  $\beta$ .

In the following sections we will determine the contribution of the various waves to the vorticity flux feedback and identify the angle  $\vartheta$  that produces the most significant contribution to this feedback. We will also calculate the feedback factor  $f_r$  as a function of the mean flow wavenumber  $n$  for  $0 \leq \varphi \leq 90^\circ$ . We will limit our discussion to the emergence of mean flows with  $n < 1$ , i.e. with scale larger than the scale of the forcing. In section 4 the analysis is mostly focused to isotropic forcing ( $\mathcal{G} = 1$ ) while the effect of anisotropy is discussed in section 5.

#### 4. Eddy-mean flow dynamics leading to formation of zonal and non-zonal structures for isotropic forcing

##### a. Induced vorticity fluxes when $\beta \ll 1$

We expand the integrand  $\mathcal{F}$  of (20) in powers of  $\beta$ :

$$\mathcal{F} = \mathcal{F}_0 + \beta^2 \mathcal{F}_2 + \mathcal{O}(\beta^4) \quad (22)$$

with  $\mathcal{F}_2 = \frac{1}{2} \partial_{\beta\beta}^2 \mathcal{F} \Big|_{\beta=0}$ . The leading order term,  $\mathcal{F}_0$ , is the contribution of each wave with wavevector  $\mathbf{k} = (\cos \vartheta, \sin \vartheta)$  to the vorticity flux feedback in the absence of  $\beta$  and is shown in Fig. 4a. For  $\beta = 0$ , the dynamics are rotationally symmetric and for isotropic forcing  $f_r$  is independent of  $\varphi$ . Therefore all zonal and non-zonal eigenfunctions with the same wavenumber,  $n$ , grow at the same rate. Upgradient fluxes ( $\mathcal{F}_0 > 0$ ) to a mean flow with wavenumber  $n$  are induced by waves with phase lines inclined at angles satisfying  $4 \sin^2 \vartheta < 1 + n^2$  (cf. Appendix B). This implies that all waves with  $|\vartheta| < 30^\circ$  necessarily produce upgradient vorticity fluxes to any mean flow with wavenumber  $n < 1$ , while  $30^\circ < |\vartheta| < 45^\circ$  produce upgradient fluxes for any mean flow with large enough wavenumber (cf. Fig. 4a). The eddy-mean flow

<sup>3</sup>While the phase speed of the marginally unstable non-zonal structures almost matches the corresponding Rossby phase speed for  $\beta \gg 1$  it overestimates the Rossby phase speed by almost by a factor of 2 when  $\beta \sim \mathcal{O}(1)$  or smaller. However, at these values of  $\beta$  we have found that the results presented in this work are not sensitive to the value of the frequency.

dynamics was investigated in the limit of  $n \ll 1$  by [Bakas and Ioannou \(2013b\)](#). It was shown that the vorticity fluxes can be calculated from time averaging the fluxes over the life cycle of an ensemble of localized stochastically forced wavepackets initially located at different latitudes. For  $n \ll 1$ , the wavepackets evolve in the region of their excitation under the influence of the infinitesimal local shear of  $\delta U$  and are rapidly dissipated before they shear over. As a result, their effect on the mean flow is dictated by the instantaneous (with respect to the shear time scale) change in their momentum fluxes. Any pair of wavepackets having a central wavevector with phase lines forming angles  $|\vartheta| < 30^\circ$  with the  $y$  axis surrender instantaneously momentum to the mean flow and reinforce it, whereas pairs with  $|\vartheta| > 30^\circ$  gain instantaneously momentum from the mean flow and oppose jet formation. Therefore, anisotropic forcing that injects significant power into Fourier components with  $|\vartheta| < 30^\circ$  (such as the forcing from baroclinic instability that primarily excites Fourier components with  $\vartheta = 0$ ) produces robustly upgradient fluxes that asymptotically behave antidiffusively. That is, for a sinusoidal mean flow perturbation  $\delta U = \sin(ny)$  we have  $\int_0^\pi \mathcal{F}_0 d\vartheta = Kn^2$  with  $K$  positive and proportional to the anisotropy factor  $\mu$  (cf. Appendix B and [Bakas and Ioannou \(2013b\)](#)).

For isotropic forcing the net vorticity flux produced by shearing of the perturbations vanishes, i.e.  $\int_0^\pi \mathcal{F}_0 d\vartheta = 0$ , given that the upgradient fluxes produced by waves with  $|\vartheta| < 30^\circ$  exactly balance the downgradient fluxes produced by the waves with  $|\vartheta| > 30^\circ$ . However, a net vorticity flux feedback is produced and asymptotically behaves as a negative fourth order hyperdiffusion with coefficient  $\mathcal{O}(\beta^2)$  for  $\beta \ll 1$  (cf. (23) and [Bakas and Ioannou \(2013b\)](#)). In Appendix B it is shown that the feedback factor  $f_r$  for isotropic forcing in the limit  $\beta \ll 1$  with  $\beta/n \ll 1$  is:

$$f_r = \beta^2 \frac{n^4}{64} [2 + \cos(2\varphi)] + \mathcal{O}(\beta^4), \quad (23)$$

which is accurate even up to  $n \approx 1$ , as shown in Fig. 5 plotting  $f_r$  as a function of  $n$ . In order to understand the contribution of  $\beta$  to the vorticity flux feedback, we plot  $\mathcal{F}_2/n^4$  for a zonal (Fig. 4b) and a non-zonal perturbation (Fig. 4c) as a function of the mean flow wavenumber  $n$  and wave angle  $\vartheta$ . We choose to scale  $\mathcal{F}_2$  by  $n^4$  because in (23)  $f_r$  increases as  $n^4$ . Consider first the case of a zonal jet. It can be seen that at every point,  $\mathcal{F}_2$  has the opposite sign to  $\mathcal{F}_0$  and assumes increasingly positive values in the range  $\vartheta \approx 58^\circ$  to  $\vartheta \approx 90^\circ$  as  $n$  increases, so that the net contribution from all angles is always positive for all  $n$  and  $\mu$  (cf. (23) for the isotropic case).

The asymptotic analysis in [Bakas and Ioannou \(2013b\)](#), which is formally valid for  $n \ll 1$ , offers understanding of the dynamics that lead to inequality  $\mathcal{F}_2 \mathcal{F}_0 < 0$  and to the positive net contribution of  $\mathcal{F}_2$ , i.e. to  $\int_0^\pi \mathcal{F}_2 d\vartheta >$

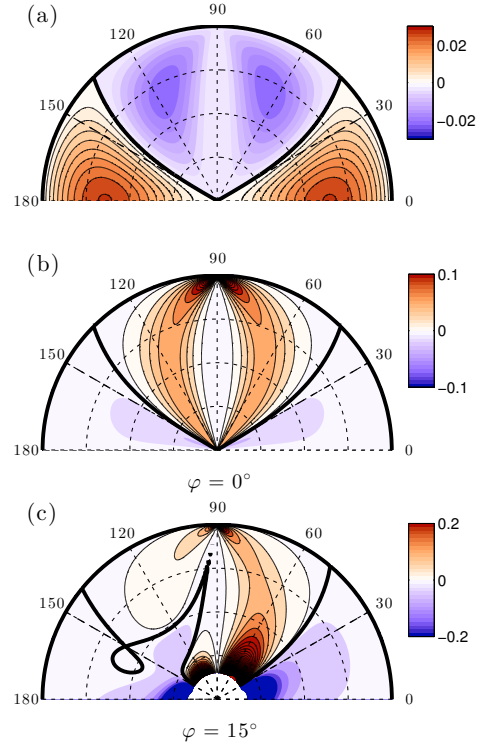


FIG. 4. (a) Contours of  $\mathcal{F}_0(\vartheta, n)$  in a  $(\vartheta, n)$  polar plot ( $n$  radial and  $\vartheta$  azimuthal) for  $\beta = 0$ . Positive values of  $\mathcal{F}_0$  that are denoted by solid lines, indicate the waves with phase lines oriented at an angle  $\vartheta$  with respect to the  $y$  axis that reinforce jet perturbations of wavenumber  $n$ . (b) Contours of  $\mathcal{F}_2(\vartheta, n)/n^4$  that gives the  $\mathcal{O}(\beta^2)$  contribution of the forced waves to the vorticity flux feedback induced by zonal jets ( $\varphi = 0$ ) and scaled appropriately. (c) Same as (b) but for non-zonal perturbations with  $\varphi = 15^\circ$ . In all panels solid lines mark positive contours and the thick line marks the contour of zero feedback. For (a) and (b) the zero contour is the curve  $4 \sin^2 \vartheta = 1 + n^2$  (see Appendix B). The radial grid interval is  $\Delta n = 0.25$ .

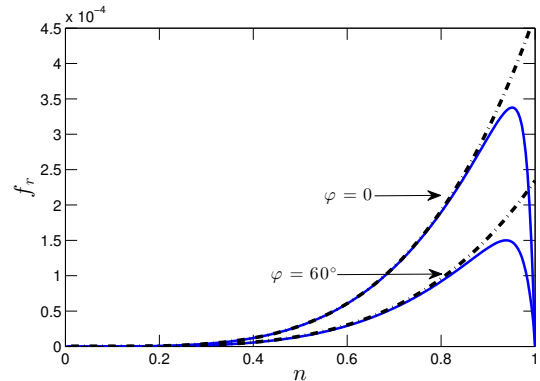


FIG. 5. Vorticity flux feedback factor  $f_r$  as a function of  $n$  for  $\beta = 0.1$  and isotropic forcing. Positive values correspond to upgradient fluxes. Shown is  $f_r$  for  $\varphi = 0$  and  $\varphi = 60^\circ$  (solid lines), as well as the asymptotic expression (23) (dash-dot) derived for the feedback factor in the limit  $\beta \ll 1$  and  $\beta/n \ll 1$ .

0. Any pair of wavepackets with wavevectors at angles  $|\vartheta| > 30^\circ$  instantaneously gain momentum from the mean flow as described above (i.e.  $\mathcal{F}_0 < 0$  for  $|\vartheta| > 30^\circ$ ), but their group velocity is also increased. This occurs due to the fact that shearing changes their meridional wavenumber and consequently their group velocity. As a result, the wavepackets flux momentum from northern latitudes, compared to when they move in the absence of the mean flow. The instantaneous change in the momentum fluxes resulting from this speed up of the wavepackets is positive in their region of excitation leading to upgradient fluxes ( $\mathcal{F}_2 > 0$ ). The opposite happens for pairs with  $|\vartheta| < 30^\circ$ , however the downgradient fluxes produced are smaller than the upgradient fluxes, leading to a net positive contribution when integrated over all angles. Figure 4b, shows that this result is valid for larger mean flow wavenumbers as well.

Consider now the case of a non-zonal perturbation (Fig. 4c). We observe that the angles for which the waves have significant positive or negative contributions to the vorticity flux feedback are roughly the same as in the case of zonal jets. In addition, the vorticity flux feedback factor for  $\varphi \neq 0$  behaves as in the case of the zonal jets and the feedback factor monotonically decreases with the angle  $\varphi$  of the non-zonal perturbations (cf. (23)). As a result, zonal jet perturbations always produce larger vorticity fluxes compared to non-zonal perturbations and are therefore the most unstable in the limit  $\beta \ll 1$ . Additionally, these results show that for  $\beta \ll 1$ , the mechanism for structural instability of the non-zonal structures is the same as the mechanism for zonal jet formation, which is shearing of the eddies by the infinitesimal mean flow.

### b. Induced vorticity fluxes when $\beta \gg 1$

Consider first the emergence of non-zonal structures in the limit  $\beta \gg 1$ . The contribution of each Fourier component of the forcing to the vorticity flux feedback  $\mathcal{F}$  for the case of non-zonal structures at  $\beta = 200$  is shown in Fig. 6a. In contrast to the cases with  $\beta \ll 1$  (or  $\beta = \mathcal{O}(1)$ , discussed in section 4c), there is only a small band of Fourier components that contribute significantly to the vorticity flux feedback, as indicated with the narrow tongues in Fig. 6a. The reason for this selectivity in the response is that for  $\beta \gg 1$  the components that produce appreciable fluxes, as seen from (21), are concentrated on the  $(\vartheta, n)$  curves that satisfy  $\mathcal{D}_2 = 0$  (shown in Fig. 6b) or equivalently for the  $(\vartheta, n)$  that satisfy the resonant condition  $\omega_{\mathbf{k}} + \omega_{\mathbf{n}} = \omega_{\mathbf{k}+\mathbf{n}}$  (cf. (A9)). That is, the resonant condition is satisfied when a Rossby wave with wavevector  $\mathbf{k}$  and frequency  $\omega_{\mathbf{k}}$  forms a resonant triad with the non-zonal structure with wavevector  $\mathbf{n}$  and frequency  $\omega_{\mathbf{n}}$ . We call these the ‘resonant contributions’ to the vorticity flux feedback.

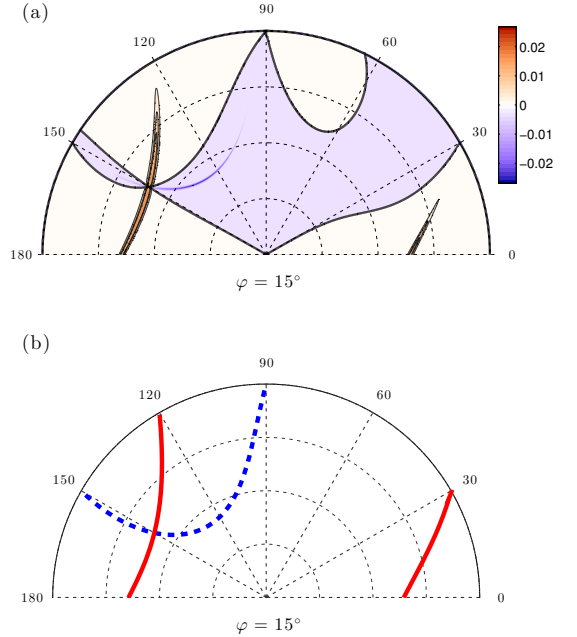


FIG. 6. (a) The contribution  $\mathcal{F}(\vartheta, n)$  of the forced waves with angle  $\vartheta$  to the vorticity fluxes induced by a non-zonal with mean flow wavenumber  $n$  and  $\varphi = 15^\circ$ . Shown are contours of  $\mathcal{F}(\vartheta, n)$  for  $\beta = 200$  ( $n$  radial and  $\vartheta$  azimuthal). Solid lines mark positive contours and the thick line marks the zero contour. (b) Zero contours of  $\mathcal{D}_2(\vartheta, n)$  in a  $(\vartheta, n)$  polar plot for non-zonal perturbations with  $\varphi = 15^\circ$  as in (a). Solid (dashed) lines correspond to upgradient (downgradient) vorticity fluxes. The radial grid interval in both panels is  $\Delta n = 0.25$ .

Resonant triads do not occur for all mean flow perturbations  $\mathbf{n}$ . For  $(n, \varphi)$  in region D of Fig. 7a,  $\mathcal{D}_2$  has no roots and therefore there are no Fourier components with  $\mathbf{k} = (\cos \vartheta, \sin \vartheta)$  that form a resonant triad with the mean flow perturbation  $\mathbf{n}$  and the vorticity flux feedback is determined by the sum over the non-resonant contributions as illustrated in Fig. 7b. In region B of Fig. 7a, there are only two resonant angles  $\vartheta$ . The resonant and non-resonant contribution for a typical case in region B is shown in Fig. 7c. Note that it is the resonant contributions that determine the vorticity flux feedback. However, they produce a negative vorticity flux feedback (a downgradient tendency), which is stabilizing, a result that holds for all  $(n, \varphi)$  in region B. In regions A and C, there exist four resonant angles  $\vartheta$  which dominate the vorticity flux. In C all resonant contributions are stabilizing and therefore C is also a stable region. In region A, which at most extends to  $\varphi = 60^\circ$  (cf. Appendix B), two of the four resonances give positive contributions to  $f_r$  (cf. Figs. 7d,e). Therefore only for  $(n, \varphi)$  in region A, does a destabilizing vorticity flux feedback occur. The largest destabilizing feedback occurs when the positively contributing resonances are near coa-



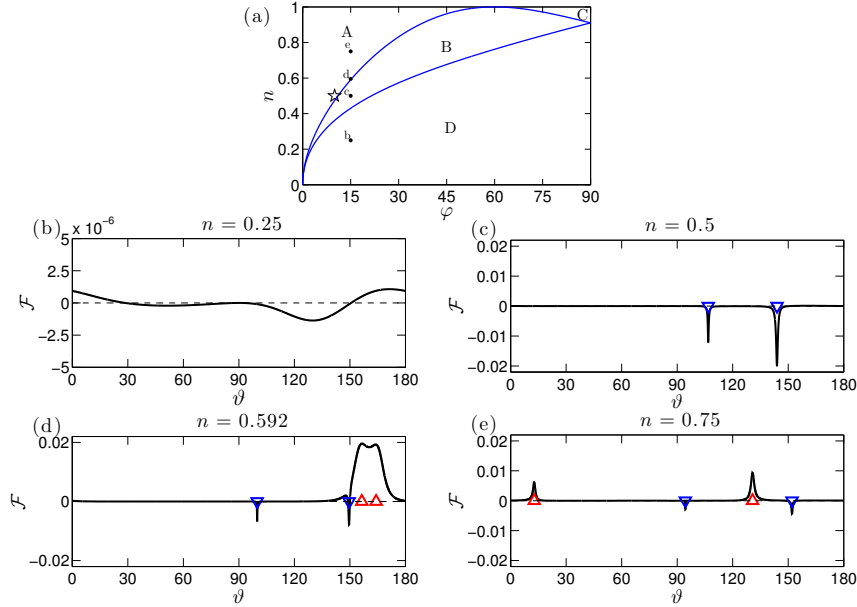


FIG. 7. (a) The curves separating the regions in the  $(n, \varphi)$  plane for which  $\mathcal{D}_2$  has no roots (region D), 2 roots (region B) and four roots (regions A and C). Only two of the roots of  $\mathcal{D}_2$  found in region A give upgradient resonant contributions to  $f_r$ . (b)–(d) The contribution  $\mathcal{F}$  to the total vorticity flux feedback from the individual waves excited by the forcing, as a function of wave angle  $\vartheta$  at  $\beta = 200$  and for a non-zonal perturbation with  $\varphi = 15^\circ$ . The mean flow wavenumber is (b)  $n = 0.25$  (in region D), (c)  $n = 0.5$  (in region B), (d)  $n = 0.592$  (in region A) and (e)  $n = 0.75$  (in region A). The resonant angles (i.e. the roots of  $\mathcal{D}_2$ ) are marked by upper (lower) triangles when the forced waves produce upgradient (downgradient) fluxes. Note that the scale in (b) is much smaller.

lence (i.e. as in Fig. 7d), which occurs for  $(n, \varphi)$  close to the curve separating regions A and B. The reason is that when the resonances are apart, as in Figs. 7c,e, the width of the resonances is  $\mathcal{O}(1/\beta)$  and the integrated resonant contributions to the vorticity flux are  $\mathcal{O}(1/\beta)$ . However, when the resonances are near coalescence, as for the case shown in Fig. 7d, the width of the resonances increases as they assume a double humped shape and, as shown in Appendix B, the destabilizing vorticity flux feedback becomes  $\mathcal{O}(1/\sqrt{\beta})$ .

It can be shown (cf. Appendix B) that the resonant contribution for  $\beta \gg 1$  asymptotically approaches

$$f_r^{(R)} = \frac{1}{\sqrt{\beta}} \sum_{j=1}^{N_r} \frac{\pi \mathcal{N}_j \eta_j}{2 \mathcal{D}_{0,j}^{1/2} |\lambda_j|^{1/2}}, \quad (24)$$

where the subscript  $j$  functions at the  $j$ -th out of the  $N_r$  roots of  $\mathcal{D}_2$  and  $\lambda = \partial_{\varphi}^2 \mathcal{D}_2$ . The values  $\mathcal{N}_j$ ,  $\mathcal{D}_{0,j}$ ,  $\lambda_j$  are all  $\mathcal{O}(1)$ , whereas  $\eta_j$  is always positive and the only quantity that has dependence on  $\beta$ . It is  $\mathcal{O}(1)$  only for  $(n, \varphi)$  just above the separating boundaries of regions A and B and regions B and D in Fig. 7a yielding  $f_r^{(R)} \sim 1/\sqrt{\beta}$  and is  $\mathcal{O}(1/\sqrt{\beta})$  elsewhere, yielding  $f_r^{(R)} \sim 1/\beta$ , as also qualitatively described above. The sign of the  $j$ -th resonant contribution to the total vorticity flux feedback depends

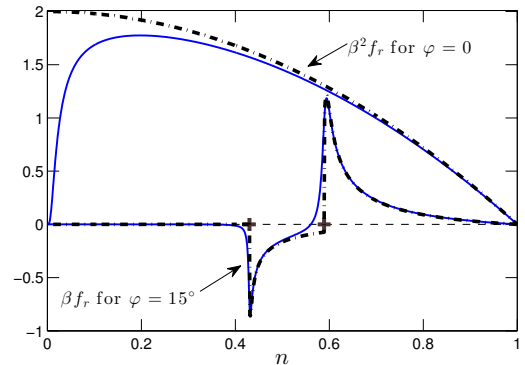


FIG. 8. Vorticity flux feedback  $f_r$  as a function of  $n$  for  $\beta = 200$ . Positive (negative) values correspond to upgradient (downgradient) fluxes. Shown is  $f_r$  for  $\varphi = 0$  (multiplied by  $\beta^2$ ) and for  $\varphi = 15^\circ$  (multiplied by  $\beta$ ). Also the asymptotic expressions (B18) for  $\varphi = 0$  and (24) for  $\varphi = 15^\circ$  are shown (dash-dot). The crosses mark the mean flow wavenumbers  $n = 0.43$  and  $n = 0.59$  that separate regions A, B and D in Fig. 7a for  $\varphi = 15^\circ$ .

only on the sign of  $\mathcal{N}_j$ . For  $(n, \varphi)$  just above the boundary separating regions B and D,  $\mathcal{N}_j < 0$  and  $f_r$  attains its minimum value, which corresponds to the largest stabilizing tendency. This is illustrated in Fig. 8, showing the flux feedback  $f_r$  as a function of  $n$ . For  $(n, \varphi)$  just above

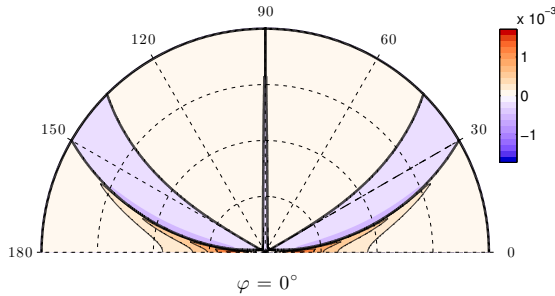


FIG. 9. Contours of  $\mathcal{F}(\vartheta, n)$  ( $n$  radial and  $\vartheta$  azimuthal) for zonal jet perturbations ( $\varphi = 0$ ) and  $\beta = 100$ . Solid lines mark positive contours and the thick line marks the zero contour. The radial grid interval is  $\Delta n = 0.25$ .

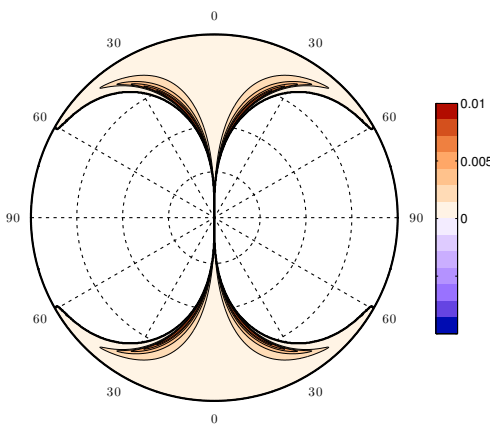


FIG. 10. Contours of the feedback factor  $f_r$  for the case  $\beta = 200$  as a function of  $n$  and  $\varphi$  ( $n$  radial and  $\varphi$  azimuthal). Shown are positive contours, so the white area corresponds to negative values indicating downgradient vorticity fluxes. The radial grid interval is  $\Delta n = 0.25$ . Note that the feedback factor is always negative (downgradient fluxes) for  $\varphi \geq 60^\circ$  (cf. Appendix B).

the boundary separating regions A and B, coalescence of the two positive contributing resonances occurs and  $f_r$  attains its maximum value, which corresponds to the largest destabilizing tendency. For small mean flow wavenumbers  $n$  (corresponding to region D) the feedback factor is negative and  $\mathcal{O}(\beta^{-2})$  due to the absence of resonant contributions.

An interesting exception to the results discussed above occurs for the important case of zonal jet perturbations ( $\varphi = 0$ ). In that case,  $\mathcal{N}_j = 0$  in (24) as the roots of  $\mathcal{D}_2$  and  $\mathcal{N}$  coincide and the resonant contribution (24) is exactly zero. As shown in Fig. 9, positive vorticity flux feedback is obtained from a broad band of the non-resonant Fourier components with  $\vartheta \approx 0^\circ$ , corresponding to waves with lines of constant phase nearly aligned with the  $y$  axis (remember that for smaller  $\beta$  the region that produces destabilizing fluxes extends up to  $|\vartheta| \approx 30^\circ$ ).

For large  $\beta$  the vorticity flux  $f_r$  is always destabilizing for all zonal jet perturbations with  $n < 1$ , as shown by (B18) and Fig. 8, and the largest destabilizing vorticity flux,  $f_{r,\max} = (2 + \mu)\beta^{-2}$ , is obtained for jets with the largest allowed scale. The reason for the weak fluxes and the preference for the emergence of jets of the largest scale in this limit is understood by noting that the stochastically forced eddies for  $\beta \gg 1$  propagate with  $\mathcal{O}(\beta)$  group velocities. Therefore in contrast to the limit of  $\beta \ll 1$  in which they evolve according to their local shear, the forced waves will respond to the integrated shear of the sinusoidal perturbation over their large propagation extent, which will be very weak.

To summarize: Although zonal jets and most non-zonal perturbations induce fluxes that decay as  $1/\beta^2$  for large  $\beta$ , resonant interactions arrest the decay rate of certain non-zonal perturbations by a factor of  $\mathcal{O}(\beta^{3/2})$  leading to fluxes that decay as  $1/\sqrt{\beta}$ . This makes the non-zonal perturbations to be the most S3T unstable perturbations for  $\beta \gg 1$ . Also in contrast to  $\beta \ll 1$  when  $f_r$  is positive for all  $n$  and  $\varphi$  (cf. Fig. 5), the vorticity flux feedback is negative for  $(n, \varphi)$  in regions B and D of Fig. 7a. As a result, the mean flows that produce negative fluxes and are by necessity S3T stable are interestingly in the interior of the dumbbell shown in Fig. 10, illustrating  $f_r$  in a polar  $(n, \varphi)$  plot. The largest destabilizing fluxes occur in the narrow region adjacent to the outer boundaries of the dumbbell shape, which demarcates the boundary separating regions A and B. Because of the selectivity of the resonances these results do not depend on the forcing anisotropy as we will see in the next section.

### c. Induced vorticity fluxes for $\beta \sim \mathcal{O}(1)$

We have seen that in the singular case of isotropic forcing the only process available for the emergence of mean flows is the fourth order antidiffusive vorticity feedback induced by the variation of the group velocity of the forced eddies due to the mean flow shear. For  $\beta \ll 1$ , the waves interact with the local shear producing fluxes proportional to  $\beta^2 d^4 \delta U / dy^4$ . As  $\beta$  increases this growth is reduced since the waves interact with an effective integral shear within their propagation extent which is weak and eventually, as we have seen in the previous section, for  $\beta \gg 1$  the fluxes decay as  $\beta^{-2}$ . Therefore, the fluxes attain their maximum at an intermediate value of  $\beta$ . This occurs for  $\beta \approx 3.5$ , as can be seen in Fig. 11a where the maximum  $f_r$  over all  $(n, \varphi)$  is shown. It will be demonstrated in the next section that this intermediate  $\beta$  maximizes the S3T instability irrespective of the spectrum of the forcing.

While the eddy–mean flow interaction of both zonal and non-zonal perturbations is dominated by the same dynamics when  $\beta \ll 1$ , for  $\beta \gg 1$  the eddy–non-zonal flow interaction is dominated by resonances which are not possible when the mean flow perturbation is zonal. The resonant

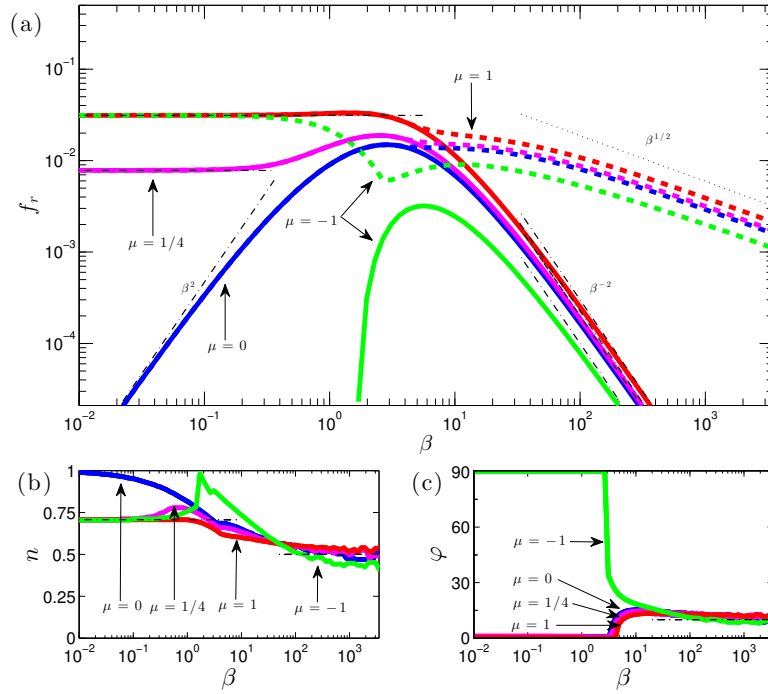


FIG. 11. The maximum value of  $f_r$  over all wavenumbers  $n$  for zonal jets (solid), and the maximum value of  $f_r$  over all wavenumbers  $n$  and angles  $\varphi \neq 0$  for non-zonal perturbations (dashed) as a function of the planetary vorticity,  $\beta$  for the three forcing covariance spectra seen in Fig. 2. Also shown are the asymptotic expressions (B4), (B6) and (B19) (dash-dot) and the  $\beta^{-1/2}$  slope (dotted). For  $\mu = -1$  zonal jet perturbations emerge for  $\beta > 1.67$ . (b) The mean flow wavenumber  $n$  and (c) the angle  $\varphi$  for which the maximum value of  $f_r$  (shown in (a)) is attained. The asymptotes  $n = 1/\sqrt{2}$  for  $\beta \ll 1$  and  $n = 0.5$ ,  $\varphi = 10^\circ$  for  $\beta \gg 1$  are also shown (dash-dot).

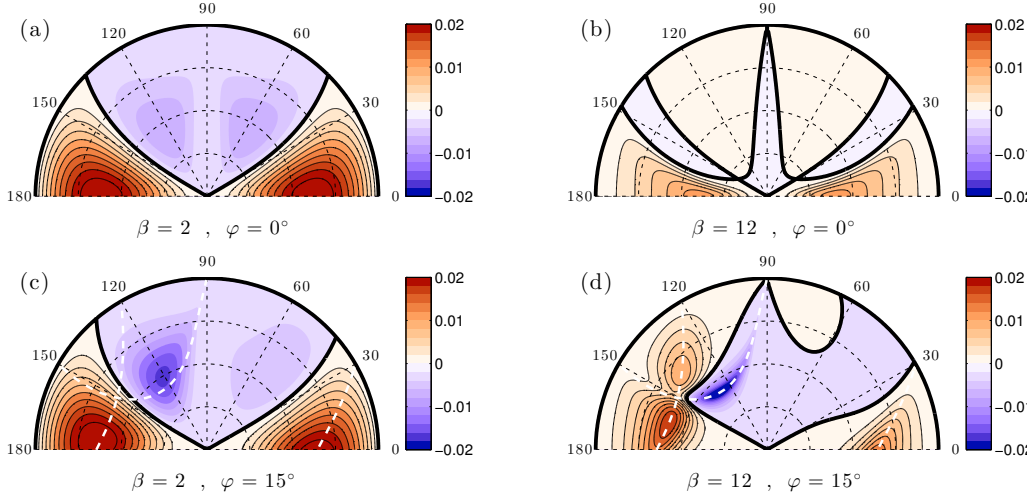


FIG. 12. Contours of the  $\mathcal{F}(\vartheta, n)$  ( $n$  radial and  $\vartheta$  azimuthal), that is the contribution of the forced waves with angle  $\vartheta$  to the vorticity fluxes induced by mean flow perturbation with mean flow wavenumber  $n$ . Shown is (a)  $\mathcal{F}$  for a zonal jet perturbation ( $\varphi = 0$ ) and (c) a non-zonal perturbation with  $\varphi = 15^\circ$  for  $\beta = 2$ . Panels (b) and (d) same as (a) and (c) for  $\beta = 12$ . Solid lines indicate positive values while thick lines mark the contour of zero feedback. White dashed lines in (c), (d) correspond to points  $(\vartheta, n)$  for which  $\mathcal{D}_2 = 0$ . The radial grid interval is  $\Delta n = 0.25$ .

interactions lead to the possibility of arrested decay of the vorticity flux at the rates of  $\beta^{-1/2}$  and  $\beta^{-1}$ , instead of the  $\beta^{-2}$  decay in the absence of resonances. The vorticity flux attains its maximum at an intermediate value  $\beta \sim \mathcal{O}(1)$  for non-zonal mean flows as well, which is nonetheless large enough for the resonant contributions to reinforce the contribution from the shearing mechanism. Figure 12 shows the contribution to the vorticity flux feedback induced by the various wave components that are excited for two values of  $\beta$  ( $\beta = 2$  and  $\beta = 12$ ) in the case of zonal jets ( $\varphi = 0$ ) and non-zonal perturbations ( $\varphi = 15^\circ$ ). As  $\beta$  increases, the resonant contributions start playing an important role for non-zonal perturbations as there is enhanced contribution to the vorticity flux feedback in the vicinity of the  $\mathcal{D}_2 = 0$  curves, indicated by the white dashed lines. These resonant contributions enhance the vorticity fluxes relative to the fluxes obtained for zonal jets and render the non-zonal structures more unstable compared to zonal jets when  $\beta \gtrsim 3.5$  (Bakas and Ioannou 2014).

### 5. Effect of anisotropic forcing on S3T instability

In this section we investigate the effect of the anisotropy of the excitation on the S3T instability. The maximum vorticity flux feedback  $f_r$  for three cases of anisotropy ( $\mu = \pm 1$  and  $\mu = 1/4$ ) and for isotropic forcing ( $\mu = 0$ ) is shown in Fig. 11a. For  $\beta \gg 1$ , the main contribution to  $f_r$  for zonal jet perturbations, comes from forced waves with nearly meridional constant phase lines (angles near  $\vartheta = 0^\circ$ , cf. Fig. 9). Therefore, the vorticity flux feedback  $f_r$ , attains larger (smaller) values for a stochastic forcing that injects more (less) power in waves with angles near  $\vartheta = 0^\circ$ , that is for positive (negative) anisotropy factor  $\mu$  (cf. Fig. 2). The maximum value of  $f_r$  over all wavenumbers  $n$  depends in this case linearly on  $\mu$  (cf. Appendix B),

$$f_{r,\max} = (2 + \mu)\beta^{-2} + \mathcal{O}(\beta^{-4}). \quad (25)$$

For non-zonal perturbations, the main contribution comes from forced waves satisfying the resonant condition  $\omega_{\mathbf{k}} + \omega_{\mathbf{n}} = \omega_{\mathbf{k}+\mathbf{n}}$  and  $f_r$  depends only on the sum of the resonant contributions. The sign of  $\mathcal{N}_j$  that determines whether the resonant contribution is positive or negative (cf. (24)), depends only on the sign of  $\sin \vartheta_j + n/2$  and not on the anisotropy factor  $\mu$  (cf. (A7c)). The anisotropy affects only the magnitude of  $\mathcal{N}_j$ . A stochastic excitation, which injects more power near  $\vartheta = 0^\circ$  ( $\mu > 0$ ) will give larger positive resonant contributions and therefore  $f_r$  increases with  $\mu$ . However, the effect on the maximum vorticity feedback is weak as the spectral selectivity of the resonances renders the characteristics of the most unstable non-zonal structure independent of the spectrum of the forcing. That is, the  $(n, \varphi)$  that correspond to the maximum  $f_r$  asymptotes to  $n \approx 0.5$ ,  $\varphi \approx 10^\circ$  (marked with star

in Fig. 7a) as  $\beta \rightarrow \infty$ , a result that is very weakly dependent on  $\mu$  (cf. Figs. 11b,c).

For  $\beta \ll 1$ , the characteristics of the S3T instability are dependent on the anisotropy of the stochastic forcing. The vorticity flux feedback is at leading order proportional to  $\mu$ :

$$f_r = \frac{1}{8}\mu n^2 (1 - n^2) \cos(2\varphi) + \mathcal{O}(\beta^2). \quad (26)$$

This shows that there can be upgradient vorticity fluxes leading to S3T instability for  $\beta = 0$  as long as  $\mu \cos(2\varphi) > 0$ . For  $\mu > 0$ , the maximum  $f_r = \mu/32$  is achieved by zonal jets ( $\varphi = 0$ ), while for  $\mu < 0$  any non-zonal perturbation with  $\varphi > 45^\circ$  can grow, with the maximum  $f_r = |\mu|/32$  achieved for  $\varphi = 90^\circ$  when the non-zonal perturbations assume the form of jets in the  $y$  direction (meridional jets) (cf. Fig. 11c).

In summary:

- a. The S3T instability of the homogeneous state is a monotonically increasing function of  $\mu$  for all  $\beta$ . The forced waves that contribute most to the instability are structures with  $\vartheta \approx 0$ , i.e. waves with phase lines nearly aligned with the  $y$  axis ( $k_y \approx 0$ ) as in Fig. 2a.
- b. The anisotropy of the excitation affects prominently the S3T stability of the homogeneous state only for  $\beta \lesssim 3.5$ .

### 6. Conclusions

The mechanism for formation of coherent structures in a barotropic beta-plane under a spatially homogeneous and temporally delta correlated stochastic forcing was examined in this work within the framework of Stochastic Structural Stability Theory (S3T). Within this framework, a second order closure for the dynamics of the flow statistics is obtained by ignoring or parameterizing the eddy-eddy nonlinearity. The resulting deterministic system for the joint evolution of the coherent flow and of the second order turbulent eddy covariance admits statistical equilibria.

For a spatially homogeneous forcing covariance, a homogeneous state with no mean coherent structures is such an equilibrium solution of the S3T dynamical system. When a critical energy input rate of the forcing is exceeded, this homogeneous equilibrium is unstable and propagating non-zonal coherent structures and/or stationary zonal jets emerge in agreement with direct numerical simulations. In order to identify the processes that lead to the formation of coherent structures, the vorticity fluxes induced by a plane wave mean flow, which is the eigenfunction of the linearized S3T system around the homogeneous equilibrium, were calculated close to the bifurcation point and closed form asymptotic expressions for these fluxes were obtained. Upgradient fluxes in this limit



are consistent with S3T instability and coherent structure formation.

The induced fluxes were calculated in a rotated frame of reference, in which the plane wave mean flow corresponds to a zonal jet evolving in a beta-plane with a tilted planetary vorticity gradient. This was done because in this rotated frame of reference the intuition gained by previous studies for the eddy–mean flow dynamics underlying zonal jet formation can be utilized to clarify the dynamics underlying non-zonal wave formation, or formation of zonal jets when the effect of topography is equivalent to a tilted planetary vorticity gradient.

In the limit of a weak planetary vorticity gradient ( $\beta \ll 1$ ), the eddy–mean flow dynamics are similar for both zonal jets and non-zonal structures. The stochastically forced eddies that propagate with low small group velocities in this limit, are rapidly dissipated as they are sheared over by the infinitesimal mean flow. Their effect on the mean flow is therefore determined at leading order by the instantaneous, with respect to the shear time scale, change in their momentum fluxes and to second order by the instantaneous change in their group velocity. The waves with constant phase lines that form angles  $|\vartheta| < 30^\circ$  with the meridional direction instantaneously surrender momentum to the mean flow and lead to upgradient fluxes that reinforce the mean flow for an anisotropic forcing. For an isotropic forcing this leading order effect produces no net fluxes when integrated over all forced waves and the instability is controlled by the second order effect that the instantaneous change of the waves’s group velocity has on the momentum fluxes. In this case, the group velocity of waves that form angles  $|\vartheta| > 30^\circ$  with the meridional direction is instantaneously increased due to refraction and the waves flux momentum from higher latitudes compared to when they move in the absence of the mean flow, resulting in upgradient fluxes. As a result, the anisotropy of the forcing has a significant effect on the induced fluxes and the S3T instability in this limit. In any case, the effect of the eddies on the mean flow due to shearing is larger for zonal jets compared to non-zonal perturbations and consequently zonal jets are more unstable in this limit.

In the limit of strong planetary vorticity gradient  $\beta \gg 1$ , the eddy–mean flow dynamics producing upgradient vorticity fluxes are different for zonal and non-zonal perturbations but in both cases the fluxes decrease with  $\beta$ . Zonal jets continue to induce upgradient vorticity fluxes through wave shearing which decrease as  $\mathcal{O}(\beta^{-2}) \ll 1$ . The reason is that in this limit the waves that can propagate in the meridional direction are influenced by the integrated shear over the sinusoidal flow, which is very small. However, the non-zonal mean flow perturbations can sustain fluxes that decrease only as  $\mathcal{O}(\beta^{-1/2})$ . The reason for these larger fluxes is that resonant and near resonant interactions dominate the dynamics in this limit (cf. section 3.26 in Pedlosky (1992)). Resonance occurs between

the emerging structure, which close to the stability boundary satisfies the Rossby wave dispersion, and the stochastically forced waves satisfying the Rossby wave frequency resonant condition. The resonant interactions which occur for non-zonal structures may produce upgradient or downgradient net fluxes and it was found that upgradient fluxes cannot be induced by non-zonal flows with wavenumbers in a region of wavenumber space in the shape of a dumbbell. Maximum upgradient fluxes occur for both zonal and non-zonal flows for  $\beta \sim \mathcal{O}(1)$ . In this regime, shearing of the forced waves by the infinitesimal non-zonal flows is reinforced by fluxes from the resonant interactions, enhancing the vorticity fluxes and rendering the non-zonal structures more unstable compared to zonal jets when  $\beta \gtrsim 3.5$ . In contrast to the limit  $\beta \ll 1$ , these results were found to be insensitive to the anisotropy of the forcing.

Finally, the relation of the S3T instability and modulational instability of finite amplitude Rossby waves was discussed in Appendix C. Parker and Krommes (2015) showed that the growth rates obtained when three Rossby waves interact with the primary finite amplitude Rossby wave, match exactly in the inviscid limit the growth rates obtained by the S3T stability analysis for the homogeneous equilibrium with the vorticity covariance produced by the primary Rossby wave. It was shown in this work that this agreement can be found for more general cases (for example when the covariance is produced by any linear combination of Rossby waves with the same total wavenumber). Such an agreement occurs because retaining only the interaction between four waves in modulational instability is equivalent to neglecting the eddy–eddy nonlinearity in S3T. The equivalence of the dynamics underlying modulational and S3T instability in this case, shows that S3T stability analysis generalizes modulational instability analysis in a stochastically forced and dissipated flow. However, the underlying S3T dynamics can capture both the emergence of large scale structure and its equilibration. In addition, the dynamics underlying modulational instability can be interpreted under the alternative eddy–mean flow view adopted in this work.

*Acknowledgments.* Nikos Bakas is supported by the AXA Research Fund and Navid Constantinou acknowledges the support of the Alexander S. Onassis Public Benefit Foundation.

## APPENDIX A

### Eddy vorticity flux response to a mean flow perturbation

In this appendix we study the eigenvalue problem (13) which determines the S3T stability of jet perturbations to the homogeneous turbulent equilibrium (7) in the rotated frame of reference. We drop the primes from the rotated

coordinates for simplicity. The eigenfunction corresponding to eigenvalue  $\sigma$  has the spatial structure:

$$\delta\tilde{U} = e^{iny}, \quad (\text{A1a})$$

$$\delta\tilde{C} = \tilde{C}_{\mathbf{n}}^{(h)}(\mathbf{x}_a - \mathbf{x}_b) e^{in(y_a+y_b)/2}. \quad (\text{A1b})$$

The power spectrum of the homogeneous part of the covariance eigenfunction,  $\tilde{C}_{\mathbf{n}}^{(h)}(\mathbf{x}_a - \mathbf{x}_b)$ , is determined from (13b) to be:

$$\begin{aligned} \hat{C}_{\mathbf{n}}^{(h)}(\mathbf{k}) &= \frac{i\varepsilon k_x}{2} [k_-^2 (k_+^2 - n^2) \hat{Q}_+ - k_+^2 (k_-^2 - n^2) \hat{Q}_-] \times \\ &\times [(\sigma + 2)k_+^2 k_-^2 + 2in\beta \cos \varphi k_x k_y - \\ &- in\beta \sin \varphi (k_x^2 - k_y^2 + n^2/4)]^{-1}, \quad (\text{A2}) \end{aligned}$$

with  $\mathbf{k}_{\pm} = \mathbf{k} \pm \mathbf{n}/2$ ,  $\mathbf{n} = (0, n)$ ,  $k = |\mathbf{k}|$ ,  $k_{\pm} = |\mathbf{k}_{\pm}|$ ,  $\hat{Q}_{\pm} = \hat{Q}(\mathbf{k}_{\pm})$  and  $\hat{Q}$  the Fourier transform of the forcing covariance (18). The vorticity flux,  $\delta\langle v'\zeta' \rangle$ , induced by this eigenfunction is

$$\begin{aligned} \delta\langle v'\zeta' \rangle &= \left[ \frac{1}{2} (\Delta_a^{-1} \partial_{x_a} + \Delta_b^{-1} \partial_{x_b}) \delta\tilde{C} \right]_{\mathbf{x}_a=\mathbf{x}_b} \\ &= in \left[ e^{in(y_a+y_b)/2} \right]_{\mathbf{x}_a=\mathbf{x}_b} \times \\ &\times \iint_{-\infty}^{+\infty} \frac{d^2\mathbf{k}}{(2\pi)^2} \left[ \frac{k_x k_y}{k_+^2 k_-^2} \hat{C}_{\mathbf{n}}^{(h)}(\mathbf{k}) e^{i\mathbf{k}\cdot(\mathbf{x}_a-\mathbf{x}_b)} \right]_{\mathbf{x}_a=\mathbf{x}_b} \\ &= \delta\tilde{U} \iint_{-\infty}^{+\infty} \frac{d^2\mathbf{k}}{(2\pi)^2} \frac{in k_x k_y}{k_+^2 k_-^2} \hat{C}_{\mathbf{n}}^{(h)}(\mathbf{k}) \equiv \varepsilon f(\sigma) \delta\tilde{U}, \quad (\text{A3}) \end{aligned}$$

which is proportional to  $\delta\tilde{U}$ . By using the symmetry  $C^e(\mathbf{x}_a, \mathbf{x}_b) = C^e(\mathbf{x}_b, \mathbf{x}_a)$ , which implies that  $\hat{C}^e(\mathbf{k}) = \hat{C}^e(-\mathbf{k})$ , and by changing the integration variable in (A3) to  $\mathbf{k} - \mathbf{n}/2$ , we obtain the following expression for the feedback factor,  $f$ :

$$\begin{aligned} f(\sigma) &= \iint_{-\infty}^{+\infty} \frac{dk_x dk_y}{(2\pi)^2} [2nk_x^2 (k_y + n/2) (k^2 - n^2)] \times \\ &\times [(\sigma + 2)k_s^2 k^2 + 2in\beta \cos \varphi k_x (k_y + n/2) \\ &- in\beta \sin \varphi (k_x^2 - k_y^2 - nk_y)]^{-1} \times \frac{\hat{Q}'(k_x, k_y)}{2}, \quad (\text{A4}) \end{aligned}$$

with  $\mathbf{k}_s = \mathbf{k} + \mathbf{n}$  and  $k_s = |\mathbf{k}_s|$ .

Introducing (A3) into (13a) we obtain the stability equation (16) that determines the eigenvalue  $\sigma$ , which can be shown to be exactly the stability equation obtained by Bakas and Ioannou (2014). The stability equation can be written in terms of the real and imaginary part of  $\sigma$  as:

$$\sigma_r = -1 + \varepsilon f_r(\sigma), \quad (\text{A5a})$$

$$\sigma_i = \beta \sin \varphi / n + \varepsilon f_i(\sigma). \quad (\text{A5b})$$

The real part of the vorticity flux feedback  $f_r$  contributes to the growth rate of the mean flow and the imaginary part  $f_i$  determines the departure of the phase speed of the mean flow from the Rossby wave frequency  $-\beta \sin \varphi / n$ . For  $\beta \gg 1$  the marginally unstable eigenfunctions have  $\sigma_i = -\omega_{\mathbf{n}} = \beta \sin \varphi / n$  as it can be readily shown that  $f_i$  is at most of  $\mathcal{O}(1)$  and therefore produces only a small correction to the Rossby phase speed which is of  $\mathcal{O}(\beta)$ .

We focus on the real part of the feedback gain,  $f_r$ , near marginal stability ( $\sigma_r \approx 0$ ). When  $f_r$  is positive, indicating upgradient vorticity fluxes, the homogeneous state is S3T unstable for  $\varepsilon > 1/f_r$ . Setting  $\sigma = -i\omega_{\mathbf{n}} = \beta \sin \varphi / n$  in (A5a) for the marginally unstable structures, we find that for the ring forcing (18),  $f_r$  can be expressed in the form:

$$f_r = \text{Re} \left( \int_0^{2\pi} \frac{\mathcal{N}}{\mathcal{D}_0 + i\beta \mathcal{D}_2} d\vartheta \right) = \int_0^{2\pi} \underbrace{\frac{\mathcal{N} \mathcal{D}_0}{\mathcal{D}_0^2 + \beta^2 \mathcal{D}_2^2}}_{F(\vartheta, n)} d\vartheta, \quad (\text{A6})$$

with  $F(\vartheta, n)$  defined by (21) and

$$\mathcal{D}_0(\vartheta, n) = 2(1 + n^2 + 2n \sin \vartheta), \quad (\text{A7a})$$

$$\begin{aligned} \mathcal{D}_2(\vartheta, n) &= (1 + n^2 + 2n \sin \vartheta) \sin \varphi / n + \\ &+ n^2 \cos(\vartheta - \varphi) + n \sin(2\vartheta - \varphi), \quad (\text{A7b}) \end{aligned}$$

$$\mathcal{N}(\vartheta, n) = \frac{1}{\pi} n (1 - n^2) \cos^2 \vartheta (\sin \vartheta + n/2) \mathcal{G}(\vartheta - \varphi). \quad (\text{A7c})$$

As Parker and Krommes (2015) noted, the stability equation (16) can be written in coordinate independent form as:

$$\begin{aligned} \sigma + 1 + i\omega_{\mathbf{n}} &= \\ &= \varepsilon \iint_{-\infty}^{+\infty} \frac{d^2\mathbf{k}}{(2\pi)^2} \frac{|\mathbf{k} \times \mathbf{n}|^2 (k_s^2 - k^2)(k^2 - n^2)}{k^4 k_s^2 n^2 [(\sigma + 2) - i(\omega_{\mathbf{k}} - \omega_{\mathbf{k}+\mathbf{n}})]} \frac{\hat{Q}(\mathbf{k})}{2}, \quad (\text{A8}) \end{aligned}$$

where  $\omega_{\mathbf{k}}$  is the Rossby frequency of a wave with wavenumber  $\mathbf{k}$  (defined in (19)). As a result in coordinate free form,

$$\beta \mathcal{D}_2(\vartheta, n) = k_s^2 (-\omega_{\mathbf{n}} - \omega_{\mathbf{k}} + \omega_{\mathbf{k}+\mathbf{n}}), \quad (\text{A9})$$

and the roots of  $\mathcal{D}_2$  on the  $(\vartheta, n)$  plane satisfy the resonant condition:

$$\omega_{\mathbf{n}} + \omega_{\mathbf{k}} = \omega_{\mathbf{k}+\mathbf{n}}. \quad (\text{A10})$$

Also note that the  $F$  defined by (21) remains unchanged when the angle  $\varphi$  is shifted by  $180^\circ$  ( $\varphi \rightarrow 180^\circ + \varphi$ ) or when there is a simultaneous shift of  $\varphi \rightarrow 180^\circ - \varphi$  and  $\vartheta \rightarrow 180^\circ - \vartheta$ . As a result, it suffices to only consider cases with  $0 \leq \varphi \leq 90^\circ$ .

## APPENDIX B

**Asymptotic expressions for the induced vorticity flux feedback**

In this Appendix we calculate in closed form asymptotic expressions for the vorticity flux feedback induced by a mean flow perturbation in the form of a zonal jet in the rotated frame of reference with wavenumber  $n$ , in the cases  $\beta \ll 1$  and  $\beta \gg 1$ .

*a. Case  $\beta \ll 1$* 

When  $\beta \ll 1$  and for  $n$  satisfying  $\beta/n \ll 1$ , we expand  $\mathcal{F}(\vartheta, n) = F(\vartheta, n) + F(180^\circ + \vartheta, n)$  in (20) in powers of  $\beta$ . Since  $\mathcal{F}$  is a function of  $\beta^2$  we have the expansion:

$$\mathcal{F} = \mathcal{F}_0 + \beta^2 \mathcal{F}_2 + \mathcal{O}(\beta^4), \quad (\text{B1})$$

with  $\mathcal{F}_2 = \frac{1}{2} \partial_{\beta\beta}^2 \mathcal{F} \Big|_{\beta=0}$ . The leading order term is:

$$\mathcal{F}_0 = \frac{n^2(1-n^2)}{\pi} \mathcal{G}(\vartheta - \varphi) \frac{1+n^2-4\sin^2\vartheta}{(1+n^2)^2-4n^2\sin^2\vartheta} \cos^2\vartheta, \quad (\text{B2})$$

due to the property  $\mathcal{G}(180^\circ + \vartheta) = \mathcal{G}(\vartheta)$ . Positive values of  $\mathcal{F}_0$  indicate that the stochastically forced waves with phase lines inclined at angle  $\vartheta$  with respect to the  $y$  direction, induce upgradient vorticity fluxes to a mean flow with wavenumber  $n$  when  $\beta = 0$ . Given that  $n < 1$  and  $\mathcal{G} > 0$ ,  $\mathcal{F}_0$  is positive for any forcing distribution, only in the sector shown in Fig. 4a in which  $4\sin^2\vartheta < 1+n^2$ . Specifically, in the absence of  $\beta$  all waves with  $|\vartheta| \leq 30^\circ$  reinforce mean flows with  $n < 1$ . Note that the condition  $4\sin^2\vartheta < 1+n^2$  is also the necessary condition for modulational instability of a Rossby wave with wavevector components  $(\cos\vartheta, \sin\vartheta)$  to any mean flow (zonal or non-zonal) of total wavenumber  $n$  for  $\beta \ll 1$  (Gill 1974).

The total vorticity flux feedback  $f_r$  for  $\mathcal{G}(\vartheta - \varphi) = 1 + \mu \cos[2(\vartheta - \varphi)]$  is at leading order:

$$f_r = \frac{\mu}{8} n^2 (1-n^2) \cos(2\varphi) + \mathcal{O}(\beta^2), \quad (\text{B3})$$

which is proportional to the anisotropy factor,  $\mu$ . The maximum feedback factor is in this case

$$f_{r,\max} = \frac{|\mu|}{32}, \quad (\text{B4})$$

and is achieved for mean flows with  $n = 1/\sqrt{2}$ . This maximum is achieved for zonal jets ( $\varphi = 0$ ) if  $\mu > 0$  and for meridional jets ( $\varphi = 90^\circ$ ) if  $\mu < 0$ . This implies that for  $\beta \ll 1$  the first structures to become unstable are zonal jets if  $\mu > 0$  and meridional jets if  $\mu < 0$ , as shown in Fig. 11c.

For isotropic forcing ( $\mu = 0$ ), the leading order term is zero and  $f_r$  depends quadratically on  $\beta$ :

$$f_r = \beta^2 \frac{n^4}{64} [2 + \cos(2\varphi)] + \mathcal{O}(\beta^4) \quad \text{for } n < 1, \quad (\text{B5})$$

producing upgradient fluxes for  $n < 1$ . Note that for the delta function ring forcing  $\int_0^{2\pi} \mathcal{F}_2 d\vartheta$  is discontinuous at  $n = 1$ , with positive values for  $n = 1^-$  and negative values for  $n = 1^+$ . The accuracy of these asymptotic expressions is shown in Fig. B13.

The maximum feedback factor, shown in Fig. 11a, is

$$f_{r,\max} = \frac{3\beta^2}{64}, \quad (\text{B6})$$

and is attained by zonal jets ( $\varphi = 0$ ) with wavenumber  $n \rightarrow 1^-$  as  $\beta \rightarrow 0$ , a result that was previously derived by Srinivasan and Young (2012). The accuracy of (B4) and (B6) extends to  $\beta \approx 0.1$ , as shown in Fig. 11a.

*b. Case  $\beta \gg 1$* 

When  $\beta \gg 1$ , we write (A6) in the form:

$$f_r = \frac{I}{\beta^2}, \quad \text{with } I = \int_0^{2\pi} F_\chi(\vartheta, n) d\vartheta, \quad (\text{B7})$$

where

$$F_\chi(\vartheta, n) = \frac{\mathcal{N} \mathcal{D}_0}{\chi^2 \mathcal{D}_0^2 + \mathcal{D}_2^2}, \quad (\text{B8})$$

and  $\chi \equiv 1/\beta$ . When  $\mathcal{D}_2 \sim \mathcal{O}(1)$  for all angles  $\vartheta$ , then the feedback factor is  $f_r \sim \mathcal{O}(\beta^{-2})$ . However, if  $\mathcal{D}_2 \sim \mathcal{O}(\beta^{-1})$  for some angle  $\vartheta$ , then as we will show in this Appendix,  $f_r$  decays as  $\mathcal{O}(\beta^{-1})$  or as  $\mathcal{O}(\beta^{-1/2})$ . This is illustrated in Fig. B13 showing the feedback factor  $f_r$  as a function of  $\beta$  in cases in which  $\mathcal{D}_2$  vanishes.

$\mathcal{D}_2$  can have at most 4 roots,  $0^\circ \leq \vartheta_j \leq 360^\circ$  ( $j = 1, 2, 3, 4$ ), for any given  $(n, \varphi)$ . At these angles the resonance condition (A10) is satisfied. To calculate asymptotic approximations to the integral  $I$ , we split the range of integration to a small range close to the roots of  $\mathcal{D}_2$  for which we have resonance,  $I^{(R)}$ , and to a range away from the roots of  $\mathcal{D}_2$ ,  $I^{(NR)}$ :

$$I = \sum_{j=1}^{N_r} \left[ \underbrace{\int_{\vartheta_{j-1}+\delta\vartheta}^{\vartheta_j-\delta\vartheta} F_\chi(\vartheta, n) d\vartheta}_{I_j^{(NR)}} + \underbrace{\int_{\vartheta_j-\delta\vartheta}^{\vartheta_j+\delta\vartheta} F_\chi(\vartheta, n) d\vartheta}_{I_j^{(R)}} \right], \quad (\text{B9})$$

where  $N_r$  is the total number of the roots of  $\mathcal{D}_2$  and  $\vartheta_0 \equiv \vartheta_{N_r}$ . Asymptotic approximations to the integral over the two ranges are then found separately using a proper

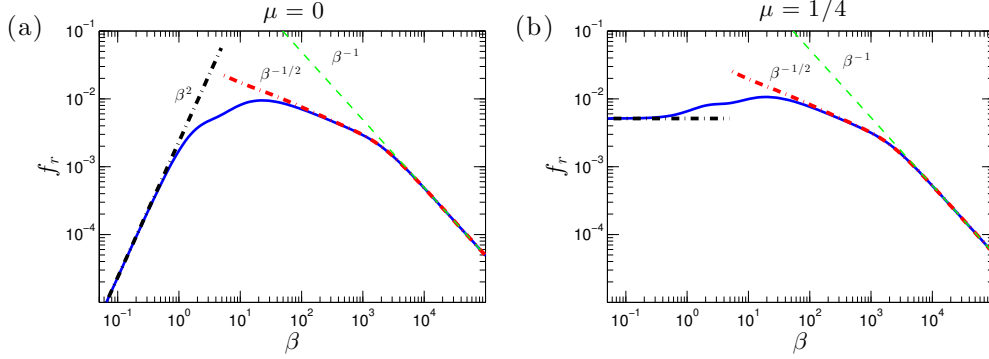


FIG. B13. Feedback factor  $f_r$  for a non-zonal perturbation with  $n = 0.4751$  and  $\varphi = 10^\circ$  (which belongs in region A of Fig. 7a) (solid lines) in the case of a forcing covariance with (a)  $\mu = 0$  and (b)  $\mu = 1/4$ . Also shown are asymptotic expressions for  $\beta \ll 1$  ((B6) in (a) and (B4) in (b)) and the resonant contribution (24) for  $\beta \gg 1$  (dash-dot). For  $\beta \gg 1$ , expression (B12) is also plotted (dashed). It can be seen that only (24) can capture the  $\beta^{-1/2}$  decrease of  $f_r$ .

rescaling for the regions close to the roots of  $\mathcal{D}_2$  (cf. Hinch (1991)).

When the distance between two consecutive roots is  $|\vartheta_j - \vartheta_{j-1}| > \sqrt{\chi}$ , as in the examples shown in Figs. 7c,e, then the dominant contribution to the integral comes from the  $\mathcal{O}(\chi)$  regions close to the roots  $\vartheta_j$ , since  $F_\chi(\vartheta, n)$  close to  $\vartheta_j$  is approximately a Lorentzian of half-width  $\mathcal{O}(\chi)$ . Therefore, choosing the range  $\delta\vartheta$  close to the roots to be  $\sqrt{\chi} \ll \delta\vartheta \ll 1$ , Taylor expanding  $F_\chi(\vartheta, n)$  close to  $\vartheta_j$  and rescaling  $\vartheta = \vartheta_j + \chi u$  we obtain:

$$I_j^{(R)} = \frac{1}{\chi} \int_{-\delta\vartheta/\chi}^{\delta\vartheta/\chi} \frac{\mathcal{N}_j \mathcal{D}_{0,j} du}{\mathcal{D}_{0,j}^2 + \mathcal{D}_{2,j}'^2 u^2} + \mathcal{O}(\chi^{-3}), \quad (\text{B10})$$

where  $\mathcal{D}_j' \equiv \partial_\vartheta \mathcal{D}_2$  and the subscript  $j$  denotes the value at  $\vartheta_j$ . In the limit  $\delta\vartheta/\chi \rightarrow \infty$  we obtain:

$$I_j^{(R)} = \frac{1}{\chi} \frac{\pi \mathcal{N}_j}{|\mathcal{D}_{2,j}'|}, \quad (\text{B11})$$

and as a result, the resonant contribution produces the asymptotic approximation:

$$f_r^{(R)} = \frac{1}{\beta} \sum_{j=1}^{N_r} \frac{\pi \mathcal{N}_j}{|\mathcal{D}_{2,j}'|}. \quad (\text{B12})$$

However, special attention should be given to the case in which two consecutive roots are close to each other. When  $|\vartheta_j - \vartheta_{j-1}| \sim \mathcal{O}(\sqrt{\chi})$  then  $\mathcal{D}_{2,j}' \sim \mathcal{O}(\sqrt{\chi})$  and  $f_r$  scales as  $1/\sqrt{\beta}$  instead of  $1/\beta$  for  $\beta \gg 1$ . Indeed, when  $F_\chi$  is double peaked, as in Fig. 7d, the dominant contribution comes from the whole range between the two resonant angles which are a distance  $\mathcal{O}(\sqrt{\chi})$  apart. The proper scaling for the angles close to  $\vartheta_j$  is therefore  $\vartheta = \vartheta_j + \sqrt{\chi}u$ . Taylor expanding the denominator under this scaling we

obtain:

$$\begin{aligned} \chi^2 \mathcal{D}_0^2 + \mathcal{D}_2^2 &= \chi^2 \mathcal{D}_{0,j}^2 + \chi \mathcal{D}_{2,j}'^2 u^2 + \chi^{3/2} \mathcal{D}_{2,j}' \mathcal{D}_{2,j}'' u^3 + \\ &+ \chi^2 \left( \frac{1}{4} \mathcal{D}_{2,j}''^2 + \frac{1}{3} \mathcal{D}_{2,j}' \mathcal{D}_{2,j}''' \right) u^4 + \mathcal{O}(\chi^{5/2}), \end{aligned} \quad (\text{B13})$$

where  $\mathcal{D}_2'' \equiv \partial_\vartheta^2 \mathcal{D}_2$  and  $\mathcal{D}_2''' \equiv \partial_\vartheta^3 \mathcal{D}_2$ . When  $\mathcal{D}_{2,j}' \sim \mathcal{O}(\sqrt{\chi})$  all the terms in (B13) are  $\mathcal{O}(\chi^2)$  and writing  $\mathcal{D}_{2,j}' = \sqrt{\chi} d(n, \vartheta_j) \equiv \sqrt{\chi} d_j$ , where  $d$  is of  $\mathcal{O}(1)$ , the leading order resonant contribution is:

$$\begin{aligned} I_j^{(R)} &= \\ &= \chi^{-3/2} \int_{-\delta\vartheta/\sqrt{\chi}}^{\delta\vartheta/\sqrt{\chi}} \frac{\mathcal{N}_j \mathcal{D}_{0,j} du}{\mathcal{D}_{0,j}^2 + d_j^2 u^2 + d_j \lambda_j u^3 + \frac{1}{4} \lambda_j^2 u^4} + \mathcal{O}(\chi^{-1}), \end{aligned} \quad (\text{B14})$$

where  $\lambda_j \equiv \mathcal{D}_{2,j}''$ . In the limit  $\delta\vartheta/\sqrt{\chi} \rightarrow \infty$  the integral can be evaluated from the residues from two of the four poles of the integrand. The two poles are at  $u = -d_j/\lambda_j \pm |z_j|^{1/2} \text{sgn}(\lambda_j) e^{\pm i w_j/2}$ , where  $|z_j| = \mathcal{D}_{0,j} |\lambda_j|^{-1} (\kappa_j^2 + 4)^{1/2}$ ,  $w_j = \arctan(2/\kappa_j)$  and  $\kappa_j \equiv d_j^2 \mathcal{D}_{0,j}^{-1} |\lambda_j|^{-1}$  is an increasing function of the distance between the two roots of  $\mathcal{D}_2$ . Therefore:

$$I_j^{(R)} = \chi^{-3/2} \frac{\pi \mathcal{N}_j \eta_j}{\mathcal{D}_{0,j}^{1/2} |\lambda_j|^{1/2}} + \mathcal{O}(\chi^{-1}), \quad (\text{B15})$$

and

$$f_r^{(R)} = \frac{1}{\beta^2} \sum_{j=1}^{N_r} \frac{1}{2} I_j^{(R)} = \frac{1}{\sqrt{\beta}} \sum_{j=1}^{N_r} \frac{\pi \mathcal{N}_j \eta_j}{2 \mathcal{D}_{0,j}^{1/2} |\lambda_j|^{1/2}}, \quad (\text{B16})$$

which is exactly (24). The factor 1/2 in (B16) arises because the range of integration includes both angles



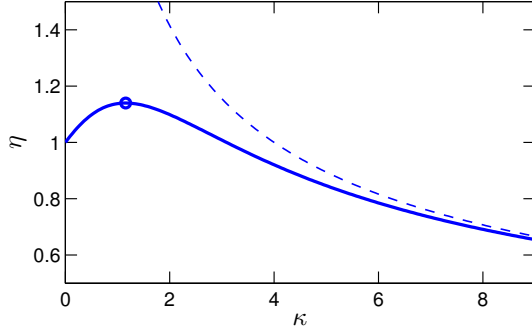


FIG. B14. The factor  $\eta = 2(\kappa^2 + 4)^{-3/4} \csc \left[ \frac{1}{2} \arctan(2/\kappa) \right]$  as a function of  $\kappa$  that is a measure of the distance between two consecutive resonant angles. The maximum value of  $\eta$  marked with an open circle (and consequently of the feedback gain that is proportional to  $\eta$ ) is  $\eta = 3^{3/4}/2 \approx 1.14$  and it is achieved at  $\kappa = 2/\sqrt{3} \approx 1.16$ . Also shown is the asymptote  $\eta = 2/\sqrt{\kappa}$  that  $\eta$  follows for  $\kappa \gg 1$  (dashed). This suggests that the resonant contribution is maximum when the two roots are very close to each other ( $\kappa \approx 1$ ) but not on top of each other ( $\kappa \ll 1$ ).

and (B15) must be divided by 2, in order to avoid double counting. The resonant response is proportional to

$$\eta = 2(\kappa^2 + 4)^{-3/4} \csc \left[ \frac{1}{2} \arctan(2/\kappa) \right], \quad (\text{B17})$$

which is always positive, because  $\kappa > 0$  as  $\mathcal{D}_0 > 0$ . The factor  $\eta$  is shown as a function of  $\kappa$  (which is a rough measure of the distance between the roots) in Fig. B14. We observe that the maximum value is attained at  $\kappa = 2/\sqrt{3} \approx 1.16$ , that is when the roots are at a distance  $\mathcal{O}(\chi^{1/2})$  apart. Note also that by taking the limit of the resonant angles being away from each other, that is by taking the limit  $\kappa \gg 1$ ,  $\eta \sim 2/\sqrt{\kappa}$  and (B16) reduces to (B12). Consequently (B16), is a valid asymptotic expression regardless of the distance between the roots  $\vartheta_j$ . The accuracy of (B12) and (B16) in comparison with the numerically obtained integral is shown in Fig. B13.

The sign of the resonant contribution depends only on the sign of  $\mathcal{N}$ . From (A7c) we see that  $\mathcal{N} > 0$  when  $\sin \vartheta > -n/2$  for  $n < 1$ ; this region is highlighted with light shading in Fig. B15. It should be noted that for the important case of zonal jet perturbations ( $\varphi = 0$ ) the resonant contribution is exactly zero because  $\mathcal{N}_j = 0$ , as shown in Fig. B15a. The asymptotic behavior of the feedback factor for this case is found from the non-resonant part of the integral. Expanding in this case the integrand for  $\chi \ll 1$ , we obtain to leading order:

$$f_r \approx f_r^{(\text{NR})} = (1 - n^2)(2 + \mu)\beta^{-2} + \mathcal{O}(\beta^{-4}), \quad (\text{B18})$$

with the maximum feedback gain

$$f_{r,\text{max}} = (2 + \mu)\beta^{-2} + \mathcal{O}(\beta^{-4}), \quad (\text{B19})$$

occurring for  $n \rightarrow 0$ . (For the special case of isotropic forcing,  $\mu = 0$ , this reduces to the result found by Srinivasan and Young (2012).)

Consider now non-zonal perturbations ( $\varphi \neq 0$ ). There is a large region in the  $(n, \varphi)$  plane (region D in Fig. 7a) in which  $\mathcal{D}_2$  has no roots and  $f_r = \mathcal{O}(\beta^{-2})$ . For larger values of  $n$  (region B in Fig. 7a), and for any given  $\varphi$ ,  $\mathcal{D}_2 = 0$  for exactly two  $\vartheta_j$  that satisfy the inequality  $\sin \vartheta_j < -n/2$ . Consequently,  $\mathcal{N}_j < 0$  and the resonant contribution from these roots is negative. For even larger values of  $n$  (regions A and C in Fig. 7a),  $\mathcal{D}_2$  has exactly 4 roots. Only two of the roots in region A produce positive resonant contributions. Note also that region A extends to  $\varphi < 60^\circ$  and  $\varphi > 120^\circ$ .

The maximum response, which is  $\mathcal{O}(\beta^{-1/2})$ , arises in region A close to the curve separating regions A and C where  $\kappa \approx 1.16$ . While the roots of  $\mathcal{D}_2$  are independent of  $\beta$ , the location and the size of the region of maximum response depends on  $\beta$  through the dependence of  $\kappa$  on  $\beta$ . However, as  $\beta$  increases this dependence is weak and as  $\beta \rightarrow \infty$  the maximum response occurs in a narrow region near  $n \approx 0.5$  and  $\varphi \approx 10^\circ$ , marked with a star in Fig. 7a. The width of this region decreases with  $\beta$ , making it exceedingly hard to locate for large  $\beta$ , and the asymptotic approach of  $(n, \varphi)$  to  $(0.5, 10^\circ)$  is shown in Fig. 11b,c.

## APPENDIX C

### Formal equivalence between the S3T instability of a homogeneous equilibrium with the modulational instability of a corresponding basic flow

Parker and Krommes (2015) have recently shown that in the inviscid limit there is a formal equivalence between the modulational instability of a Rossby wave  $\psi_{\mathbf{p}} = A \cos(\mathbf{p} \cdot \mathbf{x} - \omega_{\mathbf{p}} t)$  as studied by Lorenz (1972); Gill (1974); Connaughton et al. (2010) with the S3T instability of the homogeneous state with covariance that has the power spectrum of the Rossby wave:  $\hat{C}^e(\mathbf{k}) = (2\pi)^2 p^4 |A|^2 [\delta(\mathbf{k} - \mathbf{p}) + \delta(\mathbf{k} + \mathbf{p})]$ . The connection is formal because physically the two problems are very different. In the problem of Lorenz (1972), the stability of a basic state in the form of a coherent Rossby plane wave

<sup>4</sup>It can be shown that fluxes from the resonant contributions for  $n < 1$  are necessarily downgradient (negative) for  $60^\circ \leq \varphi \leq 120^\circ$ . Proof: A positive contribution is produced when the  $\mathcal{D}_2 = 0$  curve enters into the  $\mathcal{N} > 0$ , highlighted with light grey in Fig. B15. There are 4 roots of  $\mathcal{D}_2$  on the unit circle  $n = 1$  (on which also  $\mathcal{N} = 0$ ), at angles:  $\vartheta = 210^\circ$ ,  $270^\circ$ ,  $330^\circ$  and  $\vartheta = 90^\circ + 2\varphi$  (marked with A, B, C and D respectively). The  $\mathcal{D}_2 = 0$  curve can cross the curve AOC, which separates positive from negative  $\mathcal{N}$ , only at points A and C, since  $\mathcal{D}_2 = 0$  only at these points on AOC. Therefore, the  $\mathcal{D}_2 = 0$  curve can enter the  $\mathcal{N} > 0$  region i) through D, if it lies outside the arc ABC, and/or ii) through A, C. However, for  $60^\circ \leq \varphi \leq 120^\circ$  point D lies within the arc ABC and moreover, the gradient  $\nabla \mathcal{D}_2$  at points A and C is oriented in such way that does not allow the  $\mathcal{D}_2 = 0$  curve to enter  $\mathcal{N} > 0$ , as  $\partial_n \mathcal{D}_2 < 0$  and  $\partial_\vartheta \mathcal{D}_2 \leq 0$  ( $\partial_\vartheta \mathcal{D}_2 \geq 0$ ) at point A (point C).

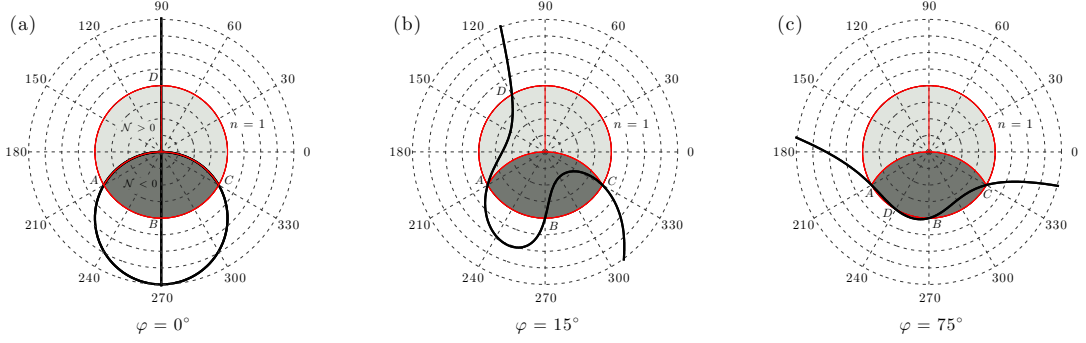


FIG. B15. Zero contours of  $\mathcal{D}_2(\vartheta, n)$  for (a) zonal jet perturbations ( $\varphi = 0$ ), (b) non-zonal perturbations with  $\varphi = 15^\circ$  and (c) non-zonal perturbations with  $\varphi = 75^\circ$  in a  $(\vartheta, n)$  polar plot. Shaded areas mark  $n \leq 1$ . Light shade corresponds to  $(\vartheta, n)$  satisfying  $\sin \vartheta > -n/2$  for which we have positive resonant contributions ( $\mathcal{N} > 0$ ), while dark areas correspond to  $\sin \vartheta < -n/2$  for which we have negative resonant contributions ( $\mathcal{N} < 0$ ). Points of intersection of the  $\mathcal{D}_2 = 0$  curve with the unit circle are marked with A, B, C, D. The radial grid interval is  $\Delta n = 0.25$ . The curve  $\mathcal{D}_2 = 0$  does not enter the  $\mathcal{N} > 0$  area for  $60^\circ \leq \varphi \leq 120^\circ$ .

is studied, while in S3T the statistical stability of an incoherent state with equilibrium covariance with the power spectrum of the Rossby wave is studied. In that sense, as noted by [Parker and Krommes \(2015\)](#), S3T stability analysis embeds the modulational instability results into a more general physical framework. In this Appendix we generalize the results of [Parker and Krommes \(2015\)](#) and show the formal equivalence between the modulational instability of any solution of the barotropic equation, which may be in general time dependent but has stationary power spectrum, with the S3T instability of the homogeneous state with the same power spectrum. For example, such a non-linear solution of the inviscid barotropic vorticity equations is a superposition of any number of Rossby waves:

$$\psi = \sum_{\substack{j=1 \\ |\mathbf{p}_j|=p}}^N A_j \underbrace{\cos(\mathbf{p}_j \cdot \mathbf{x} - \omega_{\mathbf{p}_j} t)}_{\psi_{\mathbf{p}_j}}, \quad (\text{C1})$$

all with the same total wavenumber,  $p$ , that satisfies the nonlinear barotropic equation<sup>5</sup>. Consequently it will be shown that the hydrodynamic instability of (C1) is formally equivalent with the S3T stability of the homogeneous state with spectral power:  $\hat{C}^e(\mathbf{k}) = (2\pi)^2 p^4 \sum_{j=1}^N |A_j|^2 [\delta(\mathbf{k} - \mathbf{p}_j) + \delta(\mathbf{k} + \mathbf{p}_j)]$ .

Consider a solution  $\psi_G(\mathbf{x}, t)$ , with vorticity  $\zeta_G = \Delta\psi_G$ , of the inviscid and unforced nonlinear equation (1)

<sup>5</sup>The vorticity of (C1),  $\Delta\psi = -p^2\psi$ , is proportional to  $\psi$  and as a result  $J(\psi, \Delta\psi) = 0$ . This implies that waves forced exactly on a ring can not advect each other and do not lead to a cascade. Further, waves stochastically forced with forcing covariance with spectrum  $\hat{Q}(\mathbf{k}) = 4\pi\mathcal{G}(\vartheta)\delta(k-1)$  produce a homogeneous equilibrium of the full nonlinear equations, the stability of which is governed, because of the absence of eddy-eddy interactions, exactly and not approximately by the S3T stability equations. Consequently, the critical  $\epsilon_c$  for transition to an inhomogeneous state is predicted exactly and without approximation by the S3T dynamics in the case of delta function ring forcing.

that has a time-independent power spectrum. Because  $J(\psi_G, \zeta_G) = 0$ ,  $\zeta_G$  satisfies the equation

$$\partial_t \zeta_G = \mathcal{L}^{(h)} \zeta_G, \quad (\text{C2})$$

with  $\mathcal{L}^{(h)} = -\beta \partial_x \Delta^{-1}$ . Linear perturbations  $\delta\zeta$  to this solution evolve according to the equation:

$$\partial_t \delta\zeta = \mathcal{L} \delta\zeta, \quad (\text{C3})$$

where

$$\mathcal{L} = \underbrace{-\mathbf{u}_G \cdot \nabla + (\Delta\mathbf{u}_G) \cdot \nabla \Delta^{-1}}_{\mathcal{L}'_G} \underbrace{-\beta \partial_x \Delta^{-1}}_{\mathcal{L}^{(h)}} = \mathcal{L}'_G + \mathcal{L}^{(h)}, \quad (\text{C4})$$

is the time-dependent linear operator about  $\zeta_G$  that has been decomposed into a spatially homogeneous operator,  $\mathcal{L}^{(h)}$ , that governs the evolution of  $\zeta_G$  and the inhomogeneous operator  $\mathcal{L}'_G$  that depends on  $\zeta_G$ . The stability of the solution  $\zeta_G$  is then determined by the largest Lyapunov exponent of (C3).

We decompose the perturbation into a mean  $\delta Z = \langle \delta\zeta \rangle$  and deviations from the mean  $\delta\zeta' = \delta\zeta - \delta Z$ , where  $\langle \bullet \rangle$  is an averaging operation. The averaging operation employed in modulational instability and will be employed here is projection to the non-zonal eigenstructure with wavenumber  $\mathbf{n}$ , the growth rate of which we want to determine. The solution  $\zeta_G$  has zero mean,  $\langle \zeta_G \rangle = 0$ , and therefore  $\zeta_G = \zeta'_G$ , whereas the perturbations, decomposed as  $\delta\zeta = \delta Z + \delta\zeta'$ , have non-zero mean  $\delta Z$ . Equation (C3) can then equivalently be written as:

$$\partial_t (\delta Z + \delta\zeta') = \mathcal{L}'_G \delta Z + \mathcal{L}^{(h)} \delta\zeta' + \mathcal{L}'_G \delta\zeta' + \mathcal{L}^{(h)} \delta Z, \quad (\text{C5})$$

where  $\mathcal{L}'_G$  is primed in order to stress that the operator linearly depends on the deviation quantity  $\zeta'_G$ . Equation (C5) is then separated to form an equivalent system of equations for the evolution of the mean perturbation,  $\delta Z$ , and the deviation perturbation,  $\delta\zeta'$ :

$$\partial_t \delta Z = \mathcal{L}^{(h)} \delta Z + \langle \mathcal{L}'_G \delta\zeta' \rangle \quad (\text{C6a})$$

$$\partial_t \delta\zeta' = \mathcal{L}^{(h)} \delta\zeta' + \mathcal{L}'_G \delta Z + \mathcal{L}'_G \delta\zeta' - \langle \mathcal{L}'_G \delta\zeta' \rangle. \quad (\text{C6b})$$

The stability equation (C3) and the stability equations (C6) for  $\delta Z$  and  $\delta\zeta'$  are equivalent. In modulational instability studies the term  $\mathcal{L}'_G \delta\zeta' - \langle \mathcal{L}'_G \delta\zeta' \rangle$  in (C6b) that comprises of waves with wavevectors  $\mathbf{n} \pm 2\mathbf{p}_j$ ,  $\mathbf{n} \pm 3\mathbf{p}_j, \dots$ , is neglected and the stability of the following simpler system is studied:

$$\partial_t \delta Z = \mathcal{L}^{(h)} \delta Z + \langle \mathcal{L}'_G \delta\zeta' \rangle, \quad (\text{C7a})$$

$$\partial_t \delta\zeta' = \mathcal{L}^{(h)} \delta\zeta' + \mathcal{L}'_G \delta Z. \quad (\text{C7b})$$

This truncated system, describes only the interaction between the primary waves  $\mathbf{p}_j$ , the perturbation  $\mathbf{n}$  and the waves  $\mathbf{n} \pm \mathbf{p}_j$ . In the case of  $\zeta_G$  being a single wave  $\mathbf{p}$  (as in MI studies), (C7) is referred to as the 4 mode truncation or ‘4MT’ system. However, instead of studying the stability of  $\delta Z$  and  $\delta\zeta'$  using (C7), we can equivalently study the stability of  $\delta Z$  and  $\delta C(\mathbf{x}_a, \mathbf{x}_b, t) = \langle \zeta'_G(\mathbf{x}_a, t) \delta\zeta'(\mathbf{x}_b, t) + \zeta'_G(\mathbf{x}_b, t) \delta\zeta'(\mathbf{x}_a, t) \rangle \equiv \langle \zeta'_{G,a} \delta\zeta'_b + \zeta'_{G,b} \delta\zeta'_a \rangle$ . Using (C2) and (C7b) we obtain the evolution equation for  $\delta C$ :

$$\begin{aligned} \partial_t \delta C &= \langle (\partial_t \zeta'_{G,a}) \delta\zeta'_b + (\partial_t \zeta'_{G,b}) \delta\zeta'_a + \\ &\quad + \zeta'_{G,a} (\partial_t \delta\zeta'_b) + \zeta'_{G,b} (\partial_t \delta\zeta'_a) \rangle \\ &= \left( \mathcal{L}_a^{(h)} + \mathcal{L}_b^{(h)} \right) \delta C + \\ &\quad + \langle \zeta'_{G,a} \mathcal{L}'_{G,b} \delta Z_b + \zeta'_{G,b} \mathcal{L}'_{G,a} \delta Z_a \rangle. \end{aligned} \quad (\text{C8})$$

We note from the definition of  $\mathcal{L}'_G$  (cf. (C4)) that:

$$\begin{aligned} \mathcal{L}'_G \delta Z &= (\partial_y \psi'_G) (\partial_x \delta Z) - (\partial_x \psi'_G) (\partial_y \delta Z) - \\ &\quad - (\partial_y \zeta'_G) (\partial_x \delta \Psi) + (\partial_x \zeta'_G) (\partial_y \delta \Psi) \\ &= (\Delta \delta V) (\partial_y \psi'_G) + (\Delta \delta U) (\partial_x \psi'_G) - \\ &\quad - \delta V (\partial_y \zeta'_G) - \delta U (\partial_x \zeta'_G) \\ &= (\Delta \delta \mathbf{U}) \cdot (\nabla \psi'_G) - (\delta \mathbf{U}) \cdot (\nabla \zeta'_G) = \delta \mathcal{A} \zeta'_G. \end{aligned} \quad (\text{C9})$$

where  $\delta \mathbf{U} = (\delta U, \delta V)$  is the velocity field associated with  $\delta Z$  and  $\delta \mathcal{A} = -\delta \mathbf{U} \cdot \nabla + (\Delta \delta \mathbf{U}) \cdot \nabla \Delta^{-1}$  is the operator that also appears in (8b). As a result (C8) becomes:

$$\partial_t \delta C = \left( \mathcal{L}_a^{(h)} + \mathcal{L}_b^{(h)} \right) \delta C + (\delta \mathcal{A}_a + \delta \mathcal{A}_b) C^G, \quad (\text{C10})$$

where  $C^G = \langle \zeta'_{G,a} \zeta'_{G,b} \rangle$ . Returning now to (C7a) we note that  $\langle \mathcal{L}'_G \delta\zeta' \rangle = \mathcal{R}(\delta C)$ , where  $\mathcal{R}(\delta C)$  is defined in (5),

as:

$$\begin{aligned} \mathcal{R}(\delta C) &= \\ &= -\partial_x \left[ -\frac{1}{2} (\Delta_a^{-1} \partial_{y_a} + \Delta_b^{-1} \partial_{y_b}) \langle \zeta'_{G,a} \delta\zeta'_b + \zeta'_{G,b} \delta\zeta'_a \rangle \right]_{\mathbf{x}_a = \mathbf{x}_b} \\ &\quad - \partial_y \left[ \frac{1}{2} (\Delta_a^{-1} \partial_{x_a} + \Delta_b^{-1} \partial_{x_b}) \langle \zeta'_{G,a} \delta\zeta'_b + \zeta'_{G,b} \delta\zeta'_a \rangle \right]_{\mathbf{x}_a = \mathbf{x}_b} \\ &= \langle -\partial_x (u'_G \delta\zeta' + \zeta'_G \delta u') - \partial_y (v'_G \delta\zeta' + \zeta'_G \delta v') \rangle \\ &= \langle -u'_G \partial_x \delta\zeta' - v'_G \partial_y \delta\zeta' - (\partial_x \zeta'_G) \delta u' - (\partial_y \zeta'_G) \delta v' \rangle \\ &= \langle \mathcal{L}'_G \delta\zeta' \rangle. \end{aligned} \quad (\text{C11})$$

Consequently, the hydrodynamic instability of  $\zeta'_G$  under the four mode truncation is equivalently determined from the perturbation equations:

$$\partial_t \delta Z = \mathcal{L}^{(h)} \delta Z + \mathcal{R}(\delta C) \quad (\text{C12a})$$

$$\partial_t \delta C = \left( \mathcal{L}_a^{(h)} + \mathcal{L}_b^{(h)} \right) \delta C + (\delta \mathcal{A}_a + \delta \mathcal{A}_b) C^G. \quad (\text{C12b})$$

These equations present a generalization of the modulational instability equations to basic states that comprise a large number of waves. Further, (C12) are identical to the equations that determine the S3T stability of the homogeneous equilibrium with zero mean flow,  $\mathbf{U}^e = 0$ , and equilibrium covariance  $C^e = C^G$  under the ergodic assumption that ensemble averages are equal to averages under operation  $\langle \bullet \rangle$ .

For example, consider the nonlinear solution

$$\psi(\mathbf{x}, t) = \int_0^{2\pi} a(\vartheta) \cos(\mathbf{p} \cdot \mathbf{x} - \omega_{\mathbf{p}} t) d\theta, \quad (\text{C13})$$

with wavevectors  $\mathbf{p} = (\cos \vartheta, \sin \vartheta)$  on the unit circle ( $p = 1$ ). Expanding the plane waves into cylindrical waves:

$$e^{i[(x+\beta t) \cos \theta + y \sin \theta]} = \sum_{m=-\infty}^{+\infty} i^m J_m(r) e^{im(\phi - \vartheta)}, \quad (\text{C14})$$

with  $r^2 = (x + \beta t)^2 + y^2$ ,  $\phi = \arctan [y/(x + \beta t)]$  and  $J_m$  the  $m$ -th Bessel function of the first kind, this can be shown to be the non-dispersive structure

$$\psi(x + \beta t, y) = \text{Re} \left[ \sum_{m=-\infty}^{+\infty} \gamma_m J_m(r) e^{im\phi} \right], \quad (\text{C15})$$

propagating westward with velocity  $\beta$ , where  $\gamma_m = \int_0^{2\pi} a(\vartheta) e^{-im\vartheta} d\vartheta$ . The results in this Appendix show that the modulational instability of the propagating structure (C13) is equivalent to the S3T instability of the homogeneous equilibrium with covariance  $C^e$  prescribed by power spectrum  $\hat{C}^e(\mathbf{k}) = (2\pi)^2 |a(\vartheta)|^2 \delta(k - 1)$ .

## References

- Bakas, N. A., and P. J. Ioannou, 2011: Structural stability theory of two-dimensional fluid flow under stochastic forcing. *J. Fluid Mech.*, **682**, 332–361, doi:10.1017/jfm.2011.228.
- Bakas, N. A., and P. J. Ioannou, 2013a: Emergence of large scale structure in barotropic  $\beta$ -plane turbulence. *Phys. Rev. Lett.*, **110**, 224 501, doi:10.1103/PhysRevLett.110.224501.
- Bakas, N. A., and P. J. Ioannou, 2013b: On the mechanism underlying the spontaneous emergence of barotropic zonal jets. *J. Atmos. Sci.*, **70** (7), 2251–2271, doi:10.1175/JAS-D-12-0102.1.
- Bakas, N. A., and P. J. Ioannou, 2014: A theory for the emergence of coherent structures in beta-plane turbulence. *J. Fluid Mech.*, **740**, 312–341, doi:10.1017/jfm.2013.663.
- Bernstein, J., 2009: Dynamics of turbulent jets in the atmosphere and ocean. Ph.D. thesis, Harvard University, Publication Number: AAT 3365198.
- Bernstein, J., and B. F. Farrell, 2010: Low frequency variability in a turbulent baroclinic jet: Eddy–mean flow interactions in a two-level model. *J. Atmos. Sci.*, **67** (2), 452–467, doi:10.1175/2009JAS3170.1.
- Boland, E. J. D., A. F. Thompson, E. Shuckburgh, and P. H. Haynes, 2012: The formation of nonzonal jets over sloped topography. *J. Phys. Oceanogr.*, **42**, 1635–1651, doi:10.1175/JPO-D-11-0152.1.
- Connaughton, C. P., B. T. Nadiga, S. V. Nazarenko, and B. E. Quinn, 2010: Modulational instability of Rossby and drift waves and generation of zonal jets. *J. Fluid Mech.*, **645**, 207–231, doi:10.1017/S0022112010000510.
- Constantinou, N. C., B. F. Farrell, and P. J. Ioannou, 2014: Emergence and equilibration of jets in beta-plane turbulence: applications of Stochastic Structural Stability Theory. *J. Atmos. Sci.*, **71** (5), 1818–1842, doi:10.1175/JAS-D-13-076.1.
- Danilov, S., and D. Gurarie, 2004: Scaling, spectra and zonal jets in beta-plane turbulence. *Phys. Fluids*, **16**, 2592–2603, doi:10.1063/1.1752928.
- DelSole, T., 2004: Stochastic models of quasigeostrophic turbulence. *Surv. Geophys.*, **25**, 107–149, doi:10.1023/B:GEOP.0000028160.75549.0d.
- DelSole, T., and B. F. Farrell, 1996: The quasi-linear equilibration of a thermally maintained stochastically excited jet in a quasigeostrophic model. *J. Atmos. Sci.*, **53**, 1781–1797, doi:10.1175/1520-0469(1996)053<1781:TQLEOA>2.0.CO;2.
- Di Nitto, G., S. Espa, and A. Cenedese, 2013: Simulating zonation in geophysical flows by laboratory experiments. *Phys. Fluids*, **25** (8), 086 602, doi:10.1063/1.4817540.
- Espa, S., G. Di Nitto, and A. Cenedese, 2010: The emergence of zonal jets in forced rotating shallow water turbulence: A laboratory study. *EPL*, **92**, 34 006, doi:10.1209/0295-5075/92/34006.
- Farrell, B. F., and P. J. Ioannou, 1993a: Stochastic dynamics of baroclinic waves. *J. Atmos. Sci.*, **50**, 4044–4057, doi:10.1175/1520-0469(1993)050<4044:SDOBW>2.0.CO;2.
- Farrell, B. F., and P. J. Ioannou, 1993b: Stochastic forcing of the linearized Navier-Stokes equations. *Phys. Fluids A*, **5**, 2600–2609, doi:10.1063/1.858894.
- Farrell, B. F., and P. J. Ioannou, 2003: Structural stability of turbulent jets. *J. Atmos. Sci.*, **60**, 2101–2118, doi:10.1175/1520-0469(2003)060<2101:SSOTJ>2.0.CO;2.
- Farrell, B. F., and P. J. Ioannou, 2007: Structure and spacing of jets in barotropic turbulence. *J. Atmos. Sci.*, **64**, 3652–3665, doi:10.1175/JAS4016.1.
- Farrell, B. F., and P. J. Ioannou, 2008: Formation of jets by baroclinic turbulence. *J. Atmos. Sci.*, **65**, 3353–3375, doi:10.1175/2008JAS2611.1.
- Farrell, B. F., and P. J. Ioannou, 2009a: Emergence of jets from turbulence in the shallow-water equations on an equatorial beta plane. *J. Atmos. Sci.*, **66**, 3197–3207, doi:10.1175/2009JAS2941.1.
- Farrell, B. F., and P. J. Ioannou, 2009b: A theory of baroclinic turbulence. *J. Atmos. Sci.*, **66**, 2444–2454, doi:10.1175/2009JAS2989.1.
- Galperin, B. H., S. Sukoriansky, and N. Dikovskaya, 2010: Geophysical flows with anisotropic turbulence and dispersive waves: flows with a  $\beta$ -effect. *Ocean Dyn.*, **60**, 427–441, doi:10.1007/s10236-010-0278-2.
- Gill, A. E., 1974: The stability of planetary waves on an infinite beta-plane. *Geophys. Astrophys. Fluid Dyn.*, **6**, 29–47, doi:10.1080/03091927409365786.
- Hinch, E. J., 1991: *Perturbation Methods*. Cambridge University Press.
- Ingersoll, A. P., 1990: Atmospheric dynamics of the outer planets. *Science*, **248**, 308–315, doi:10.1126/science.248.4953.308.
- Lorenz, E. N., 1972: Barotropic instability of Rossby wave motion. *J. Atmos. Sci.*, **29**, 258–269, doi:10.1175/1520-0469(1972)029<0258:BIORWM>2.0.CO;2.
- Marston, J. B., 2010: Statistics of the general circulation from cumulant expansions. *Chaos*, **20**, 041 107, doi:10.1063/1.3490719.
- Marston, J. B., 2012: Atmospheres as nonequilibrium condensed matter. *Annu. Rev. Condens. Matter Phys.*, **3**, 285–310, doi:10.1146/annurev-conmatphys-020911-125114.
- Marston, J. B., E. Conover, and T. Schneider, 2008: Statistics of an unstable barotropic jet from a cumulant expansion. *J. Atmos. Sci.*, **65**, 1955–1966, doi:10.1175/2007JAS2510.1.
- Parker, J. B., and J. A. Krommes, 2013: Zonal flow as pattern formation. *Phys. Plasmas*, **20**, 100 703, doi:10.1063/1.4828717.
- Parker, J. B., and J. A. Krommes, 2014: Generation of zonal flows through symmetry breaking of statistical homogeneity. *New J. Phys.*, **16** (3), 035 006, doi:10.1088/1367-2630/16/3/035006.
- Parker, J. B., and J. A. Krommes, 2015: Zonal flow as pattern formation. *Zonal jets*, B. Galperin, and P. L. Read, Eds., Cambridge University Press, chap. 5.
- Pedlosky, J., 1992: *Geophysical Fluid Dynamics*. 2nd ed., Springer.
- Read, P. L., Y. H. Yamazaki, S. R. Lewis, P. D. Williams, K. Miki-Yamazaki, J. Sommeria, H. Didelle, and A. Fincham, 2004: Jupiter’s and Saturn’s convectively driven banded jets in the laboratory. *Geophys. Res. Lett.*, **87**, 1961–1967, doi:10.1029/2004GL020106.
- Srinivasan, K., and W. R. Young, 2012: Zonostrophic instability. *J. Atmos. Sci.*, **69** (5), 1633–1656, doi:10.1175/JAS-D-11-0200.1.



- Srinivasan, K., and W. R. Young, 2014: Reynold stress and eddy diffusivity of  $\beta$ -plane shear flows. *J. Atmos. Sci.*, **71** (6), 2169–2185, doi:10.1175/JAS-D-13-0246.1.
- Sukoriansky, S., N. Dikovskaya, and B. Galperin, 2008: Nonlinear waves in zonostrophic turbulence. *Phys. Rev. Lett.*, **101** (1), 178 501, doi:10.1103/PhysRevLett.101.178501.
- Tobias, S. M., K. Dagon, and J. B. Marston, 2011: Astrophysical fluid dynamics via direct numerical simulation. *Astrophys. J.*, **727**, 127, doi:10.1088/0004-637X/727/2/127.
- Vallis, G. K., and M. E. Maltrud, 1993: Generation of mean flows and jets on a beta-plane and over topography. *J. Phys. Oceanogr.*, **23**, 1346–1362, doi:10.1175/1520-0485(1993)023<1346:GOMFAJ>2.0.CO;2.
- Vasavada, A. R., and A. P. Showman, 2005: Jovian atmospheric dynamics: an update after *Galileo* and *Cassini*. *Rep. Prog. Phys.*, **68**, 1935–1996, doi:10.1088/0034-4885/68/8/R06.
- Weeks, W. R., Y. Trian, J. S. Urbach, K. Ide, H. L. Swinney, and M. Ghil, 1997: Transitions between blocked and zonal flows in a rotating annulus. *Science*, **278** (5343), 1598–1601, doi:10.1126/science.278.5343.1598.